Engineered disorder in photonics

Sunkyu Yu[1,2,6], *Cheng-Wei Qiu*[3,6], *Yidong Chong*[4], *Salvatore Torquato*[5] ✉ *and Namkyoo Park*[1] ✉

Abstract | Disorder, which qualitatively describes some measure of irregularities in spatial patterns, is ubiquitous in many-body systems, equilibrium and non-equilibrium states of matter, network structures, biological systems and wave–matter interactions. In photonics, the introduction of order and disorder for device applications has traditionally been treated separately. However, recent developments in nanofabrication and design strategies have enabled the use of materials that lie between the extremes of order and disorder that can yield innovative optical phenomena owing to their engineered disordered patterns. Here, we review recent achievements in the emerging field of engineered disorder in photonics by outlining milestones in the control of the spectrum, transport, wavefront and topology of light in disordered structures. We show that engineered disorder has begun to transform the traditional landscape of photonics by introducing a greatly enhanced design freedom and, hence, has great potential for the rational design of the next generation of materials.

Order and disorder are often regarded as polar opposites. Because of the sharply distinct properties of ordered and fully random systems, the applications of ordered and disordered systems are commonly believed to be separated from each other; an example is the degraded signal-transport performance of disordered physical[1] or network[2] systems. However, 'disorder' actually encompasses an immense variety of patterns that lack long-range order. Unlike the strict definitions of order, disorder tends to be vaguely defined and is often considered challenging to manipulate.

However, the classifications and applications of disorder are increasingly being explored in a variety of research fields: examples are scale-free graphs in network science[3] and the seemingly random scatterers with crystal-analogous behaviours[4]. With the formulation of a common definition of uncorrelated disorder, we can enjoy a full spectrum of disorder that includes order, uncorrelated disorder and novel classes of correlated disorder (FIG. 1), each offering unique properties derived from engineered structural patterns. Researchers in multiple fields started to explore deliberately engineered structural patterns to achieve specific goals, such as fine-tuning wave propagation[5] or developing robust networks[2]. Notably, such efforts commonly yield structures that are not ordered but also not completely randomized in the usual sense. They, instead, occupy the rich terrain between those two conceptual extremes, simultaneously exhibiting unique advantages selectively derived from both order and uncorrelated disorder. Notable examples can be found in soft-condensed-matter physics and network theory, including hyperuniform states[4] (BOX 1), jamming transition[6] and small-world graphs[2].

In photonics, the use of structural engineering of ordered structures dates back to the analysis of multilayer films by Lord Rayleigh[7] in the 1880s. Ordered structures, including distributed Bragg reflectors, photonic crystals[8] and quasicrystals[9] (FIG. 1a,b), are now a standard toolkit for generating spatially extended optical modes or photonic bandgaps (PBGs), which allow long-range wave propagation or frequency-selective omnidirectional reflection, respectively. Most notably, photonic crystals have garnered great attention as 'semiconductors for light' that allow wide-ranging applications[8], as they can realize the wide assortment of band-structure-related features found in condensed-matter physics, including topologically nontrivial bands[10]. Wave behaviours in quasicrystals have also been explored using optical induction in photosensitive materials[11] or evanescently coupled waveguides[12]. Such photonic quasicrystals allow the transition between extended and localized modes in the absence of disorder, as demonstrated in 1D[12] and 2D[13] lattices.

By contrast, research on optical disorder started from the other extreme: uncorrelated disorder (FIG. 1h). Since Anderson's Nobel-prize-winning discovery[14] of the absence of diffusion in disordered crystals, light behaviours in disordered structures have been intensively studied, starting from absorption near a photon mobility edge[15] and weak[16] or strong localization[17,18] in uncorrelated disordered systems. Exotic optical properties inside disordered structures have also been examined in the spectral domain, as in the case of structural

✉*e-mail: torquato@princeton.edu; nkpark@snu.ac.kr*

https://doi.org/10.1038/s41578-020-00263-y

colours in complex media[19–21] and of the annihilation of PBGs[22]. Various practical applications have been realized by utilizing spatial localization or spectral broadening in disordered photonic structures, such as imaging[23], light harvesting[24] and lasing[25]. For this regime, the review article by Diederik S. Wiersma[26] provides an excellent pathway for exploiting disorder for photonics, with an interpretation based on multiple scatterings: it discusses weak and strong localization, natural disorder and the quantum nature of multiple scatterings, as well as the early works on hyperuniformity. Investigations of the regimes between perfect order and uncorrelated disorder have followed. Disordered platforms in these intermediate regimes are just starting to pave the way to nontrivial wave phenomena and photonic devices, simultaneously achieving or exceeding the advantages of ordered and highly randomized structures. Before introducing these fascinating achievements, we discuss the regimes of disordered structures between extremes, illustrating the classification of disorder.

Classification of disordered structures

The ability to engineer disorder in materials requires a capacity to classify them by quantifying their degree of order. Devising such 'order metrics' is a highly nontrivial challenge, but the tentative solutions put forth during the past two decades have been fruitfully applied to characterize a wide variety of systems, including sphere packings[27–29], simple liquids[27,30], glasses[31], water[32], random media[33] and biological systems[34]. If sensitive order metrics can be established, one can then devise experimental or numerical protocols that generate microstructures with prescribed order metrics and desirable physical properties[35].

Material structures are generally characterized by a spectrum of disorder that spans from purely uncorrelated disorder to perfect order. The extreme ends of this disorder spectrum are well understood. Crystallography tells us that a crystal is characterized by long-range translational and orientational order, which are manifested in the scattering intensity as Bragg-peak patterns (FIG. 1a and BOX 1). A quasicrystal lacks long-range translational order but possesses a long-range orientational order that is prohibited crystallographically[36,37]. Although the scattering patterns of quasicrystals exhibit Bragg peaks (FIG. 1b), these are dense and the ratios of any two Bragg-peak locations are irrational numbers, in contrast to those of crystals. On the opposite extreme of uncorrelated disorder for a statistically homogeneous system (FIG. 1h) is the Poisson distribution, which is mathematically well understood. Intermediate states within the disorder spectrum are the most difficult to define and characterize quantitatively. For example, it is unclear where in this spectrum defective crystals (FIG. 1c,d), disordered systems with short-range order (liquids and glasses) and disordered hyperuniform systems and their modifications (FIG. 1e–g) lie.

Many relevant order metrics have been devised to classify disordered structures, especially at intermediate states between order and uncorrelated disorder. Although a comprehensive discussion and classification of order metrics is beyond the scope of this Review, it is useful here to note some representative order metrics that have been identified, including the bond-orientational[38,39], translational[28,40], long-range[4,41,42] and τ order metrics[40]. Because all these order metrics have strengths and weaknesses, the question arises as to what the characteristics of a good order metric are. It has been suggested that a good order metric should have some qualitative and quantitative properties[28,29,43] (BOX 2). For example, the typical bond-orientational order metric[38,39] measures only local order and, hence, cannot capture order at intermediate and large length scales. By contrast, the Hurst exponent[42] cannot capture order at short length scales. By comparison, the τ order metric[40], which is proportional to the volume integral of $[S(\mathbf{k})-1]^2$ over the entire reciprocal space, satisfies the length-scale criterion of a good metric: quantifying the degree of disorder across all length scales[40,44,45].

Each class of disorder can lead to specific wave behaviours inside materials. In examining light–matter interactions, the identification of the relationship between order metrics and wave properties is a complex, multidimensional problem depending on a variety of wave quantities interrelated through Maxwell's equations, but one that should be pursued, in our view. The concept of order metrics has been insufficiently exploited in photonics as compared with other many-body systems — sphere packings[27,29], simple liquids[27,30] and glasses[31] — hindering research in disordered photonics; TABLE 1 lists examples of the order metrics discussed in this Review. The development and application of a well-defined set of order metrics for photonics deserves attention to fully exploit the large number of available degrees of freedom to design novel disordered photonic materials.

Engineered disorder in photonics

Light flows in disordered structures are determined by the interactions between multiple wave quantities and the many degrees of freedom inherent to disordered systems. This complexity hinders the understanding of disordered photonics. At the same time, it provides substantial design freedom for precisely controlling a set of wave properties. For example, because of the distinct expressions of each wave quantity in the wave equation, the transition from order to uncorrelated disorder does not affect each wave quantity equally, allowing for seemingly contradictory phenomena, such as narrowband resonances with broadband momentum transformation[46]. Furthermore, even at similar strengths

Author addresses

[1]Photonic Systems Laboratory, Department of Electrical and Computer Engineering, Seoul National University, Seoul, South Korea.
[2]Intelligent Wave Systems Laboratory, Department of Electrical and Computer Engineering, Seoul National University, Seoul, South Korea.
[3]Department of Electrical and Computer Engineering, National University of Singapore, Singapore, Singapore.
[4]Division of Physics and Applied Physics, School of Physical and Mathematical Sciences, Nanyang Technological University, Singapore, Singapore.
[5]Department of Chemistry, Department of Physics, Princeton Institute for the Science and Technology of Materials, Program in Applied and Computational Mathematics, Princeton University, Princeton, NJ, USA.
[6]These authors contributed equally: Sunkyu Yu, Cheng-Wei Qiu.

of perturbations of the ordered state, various patterns of disorder can lead to entirely new functionalities, as shown by the lack of PBGs in systems with uncorrelated disorder in comparison to the complete PBGs (blocking all directions and polarizations of light) in disordered hyperuniform structures[5,47].

To treat these multifaceted manifestations of disorder in photonic systems, in the following sections, we classify light–disorder interactions and the related order metrics in terms of controlled wave quantities to describe coherent design parameters and the underlying physics for each domain, and also to categorize device applications. Most importantly, this wave-quantity-based classification of disorder clarifies the concept of 'engineering' disorder: purposefully combining order and randomness to customize optical waves. FIGURE 2a illustrates the concept of engineering disorder, assuming two wave quantities, Q_p and Q_q. These generic quantities can be selected from the physical properties of photons (such as frequency, spatial mode, wavevector or topology) or from their wave properties (such as PBGs, localization, angular bandwidth or spin–orbit coupling), as shown in FIG. 2b. The state of light in the 2D space of wave quantities is then defined by the point (Q_p, Q_q).

In the simplest case of uncorrelated perturbations applied to ordered structures, we can expect the trivial transition between order and uncorrelated disorder (arrow labelled traditional disorder in FIG. 2a) with similar gradual variations of both wave quantities, such as the gradual decrease of the bandgap width and localization length with increasing perturbation. However, by exploiting the vast design freedom in disordered structures, we can find almost infinite possible loci for the transition between order and uncorrelated disorder

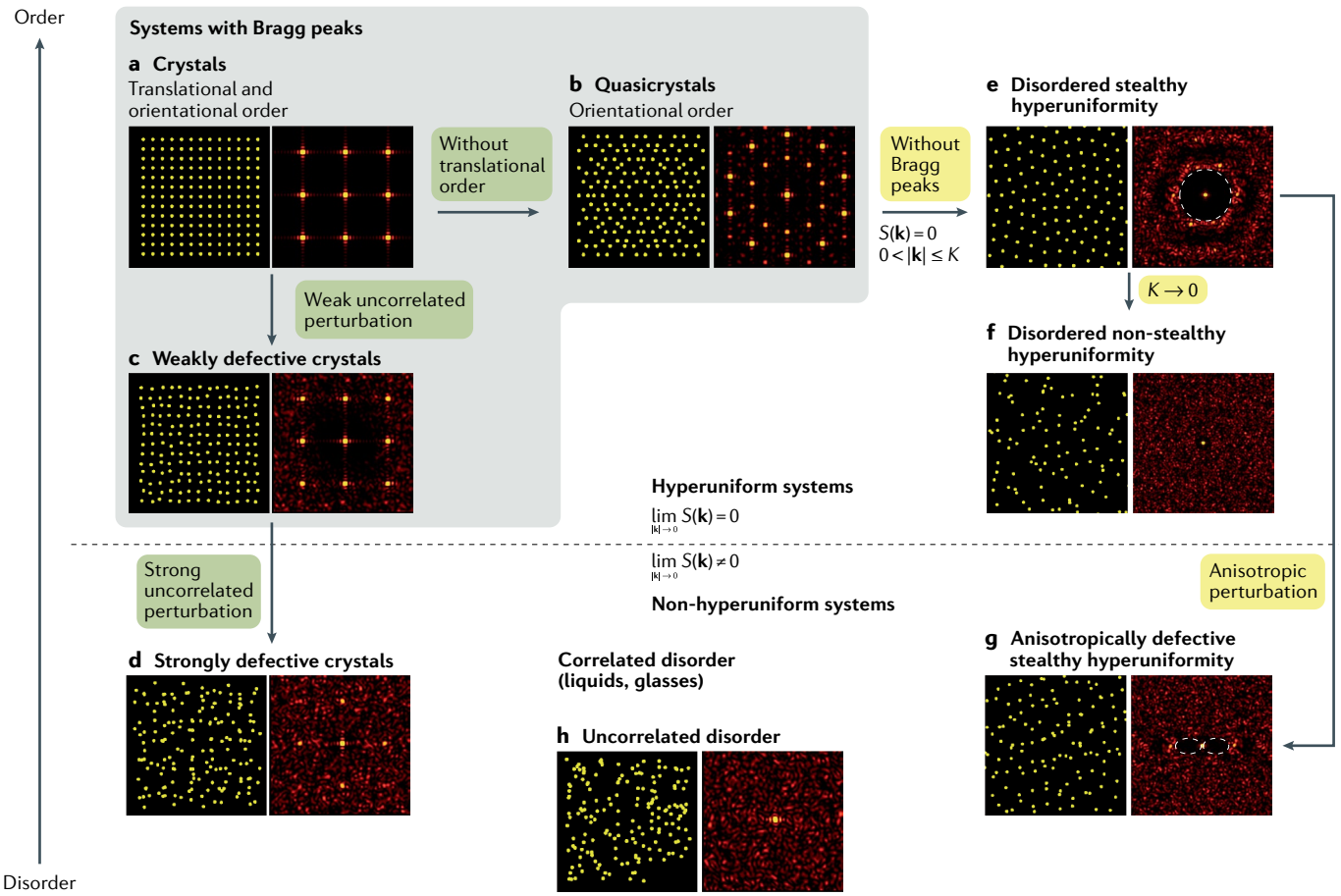

Fig. 1 | **Landscape of order and disorder.** Selected states of 2D statistically homogeneous materials organized according to their degree of disorder, from lowest to highest: crystals (panel **a**), quasicrystals[37] (panel **b**), weakly defective crystals (panel **c**), strongly defective crystals (panel **d**), disordered stealthy hyperuniform materials[50] (panel **e**), non-stealthy hyperuniform materials[4] (panel **f**), anisotropically defective stealthy hyperuniform materials (panel **g**) and uncorrelated disordered states (panel **h**). The left and right parts of each sub-panel show the particle distribution and structure factor $S(\mathbf{k})$ (BOX 1) of each state, respectively. The white dashed lines in panels **e** and **g** represent the regions of suppressed scattering. In addition to the traditional regimes of order (such as crystals and quasicrystals) and disorder (such as defective crystals) that are defined by long-range order and its breaking, indicated by the arrows with the green text boxes, the utilization of $S(\mathbf{k})$ and its associated order metrics[40,45], indicated by the arrows with the yellow text boxes, significantly extends the range of order and disorder that can be defined, including disordered hyperuniform systems and their modification. Strong perturbations in crystalline systems and designed perturbations in hyperuniform systems can lead to different forms of non-hyperuniform systems. There are also vast, undescribed regimes, including inhomogeneous[101] and dynamical systems[159]. The phenomena associated with $S(\mathbf{k})$ — Bragg peaks in crystals and quasicrystals and suppressed scattering in hyperuniform materials — are general to d-dimensional systems, though the detailed profile of $S(\mathbf{k})$ is dependent on the dimensionality, as was demonstrated for the asymptotic behaviour of $S(\mathbf{k})$ ($|\mathbf{k}| \to 0$) in hyperuniform systems[60].

Box 1 | **Hyperuniform systems**

The spatial arrangement of a system consisting of N identical particles in a volume V under periodic boundary conditions is described by the Fourier transform of the particle density: the collective density variable is defined as $\rho(\mathbf{k}) = \sum_j \exp(-i\mathbf{k}\cdot\mathbf{r}_j)$, where $\mathbf{k}$ is the wavevector and $\mathbf{r}_j$ the position of the jth particle. The structure factor is defined as $S(\mathbf{k}) = |\rho(\mathbf{k})|^2/N$ and is proportional to the intensity in elastic scattering radiations. A hyperuniform system is one in which $S(\mathbf{k})$ tends to zero as $|\mathbf{k}| \to 0$ in the thermodynamic limit ($N \to \infty$ and $V \to \infty$, such that N/V is a fixed constant), thus, suppressing infinite-wavelength density fluctuations. Because the particle 'density' determines the refractive index profile in photonics and $S(\mathbf{k})$ is proportional to the scattering intensity, hyperuniformity describes optical structures supporting the complete suppression of wave scattering as $|\mathbf{k}| \to 0$.

Stealthy hyperuniformity is a stronger form of hyperuniformity in which $S(\mathbf{k}) \sim 0$ for $|\mathbf{k}| < K$, resulting in suppressed density fluctuations from infinite wavelength down to intermediate wavelengths ($\sim 2\pi/K$, white dashed line in FIG. 1e). All crystals are stealthy, but the discovery of disordered stealthy hyperuniform systems was a remarkable development, because their scattering patterns for $|\mathbf{k}| < K$ are exactly like those of crystals and, yet, they are fully isotropic structures without any Bragg peaks. Such amorphous states are different from weakly perturbed lattices, which are anisotropic structures that generally possess Bragg peaks. Moving beyond the description of disorder in ideal gases, liquids and glasses, hyperuniformity and stealthiness generalize the notion of long-range order, enabling one to think of crystals, quasicrystals, prime numbers and certain exotic disordered systems as having this generalized long-range order.

(dashed lines in FIG. 2a). The key idea behind engineering disorder concerns the design of such loci to achieve the independent control of target wave quantities and, thus, realize a system mixing the properties of order and uncorrelated disorder (stars in FIG. 2a), such as complete and large bandgaps with perfect isotropy[5,47].

Not all the diverse facets of disordered photonics can be included in this brief Review. Our focus is on recent milestones in the field of engineered disorder, which are classified in terms of target wave quantities: spectral responses, localization and transport, wavefront shaping and topological properties. TABLE 1 summarizes the underlying physics and target wave quantities treated in this Review.

Engineered spectral responses

Ordered photonic structures exhibit distinct spectral responses, such as PBGs in crystals[8] and self-similar spectra in quasicrystals[9]. Local perturbations in ordered systems result in defect modes in the spectrum that allow for guided or resonant wave behaviours[8]. At the other extreme, the introduction of randomness in the entire structure results in chaotic and broadened spectral responses, such as the annihilation of PBGs[22] or broadband absorption[48,49]. This apparent distinction between the spectral responses of ordered and random structures has differentiated their conventional use in photonic devices.

In the intermediate regimes between order and uncorrelated disorder, engineered disorder allows for anomalous spectral responses starkly distinct from the conventional broadening in uncorrelated disorder, while keeping some wave properties typical of uncorrelated disorder. By employing approaches such as Fourier-space design[35,50], tessellation[51,52], deformation[53] and transformation[42], engineered disorder can combine the advantages of order and randomness. In this section, we exemplify the engineering of spectral responses in this intermediate regime of disorder, achieving crystal-analogous spectral responses in conjunction with random-analogous broadband momentum coupling, isotropy and localization lengths.

Chaotic channels for broadband coupling. A system is called chaotic if it is exponentially sensitive to its initial conditions. Such sensitivity originates from the onset of unstable and aperiodic states governed by deterministic laws[54]. Therefore, chaotic phenomena involve the emergence of disorder, such as broken symmetries or reduced correlations that alter symmetry-protected states. In photonics, a deformed microcavity breaking continuous rotational symmetry[53] achieves chaotic wave trajectories sensitive to initial conditions. Combined with the notion of chaotic channels, engineered disorder has provided new design freedom in the spectral and momentum domains, realizing broadband coupling to high-quality-factor resonances.

For the perturbed radius $r(\varphi) = R + \delta(\varphi)$ along the azimuthal axis φ, the degree of disorder in a deformed microcavity is solely determined by the periodic deformation $\delta(\varphi) = \delta(\varphi + 2\pi)$. For a semi-analytical approach using the Kolmogorov–Arnold–Moser theorem[53], one scalar parameter is usually applied to explore chaotic phenomena. For a limaçon structure $r(\varphi) = R(1 + \varepsilon\cos\varphi)$, the scalar parameter ε serves as an order metric, quantifying the deformation of the microcavity (TABLE 1). According to the Kolmogorov–Arnold–Moser theorem, some regular (periodic or quasiperiodic) ray dynamics survive for a sufficiently smooth microcavity deformation (for example for $\varepsilon \sim 0.1$, close to order), whereas a large deformation ($\varepsilon \sim 0.4$, close to full randomness) results in predominantly chaotic wave dynamics. In the interesting regime of moderate deformation ($\varepsilon \sim 0.3$), one can expect the emergence of engineered disorder, mixing wave properties of order (or unperturbed microcavities) and full randomness (or large deformation). Indeed, regular and chaotic wave dynamics coexist, interestingly coupled with each other by dynamical tunnelling[55], a generalized tunnelling process that includes any classically forbidden transitions. Owing to the unique properties of each regime and to dynamical tunnelling, a suitable engineering of ε enables photonic devices with totally different functionalities.

Illustrative examples of each regime and their device applications are shown in FIG. 3. Through the substantial deformation of a resonator with a D-shaped geometry (FIG. 3a), fully chaotic ray dynamics are obtained. This chaotic field interference results in a very small characteristic length of field profiles and, thus, prohibits the build-up of coherent waves, allowing for the spatiotemporal stabilization of a laser[56] with suppressed nonlinear interactions. By contrast, a very weak deformation of a resonator (FIG. 3c) that mostly conserves regular ray dynamics leads to weak dynamical tunnelling and radiation loss. The delicate balance between coupling (dynamical tunnelling) and energy transfer (radiation loss) is achieved by controlling the strength of the deformation[57], which leads to the emergence of an exceptional point: a singularity in the system parameter space at which multiple eigenvalues and their eigenmodes coalesce[58]. Because the exceptional point

results in a narrow linewidth for each coalesced eigenmode, photonic devices with ultrahigh sensitivity can be realized.

The intermediate regime of deformation (FIG. 3b) hosts coexisting regular and chaotic wave dynamics. The disorder-assisted dynamical tunnelling between 'narrowband' (order-like) resonance modes and chaotic 'broadband' (random-like) momentum channels enables the independent control of spectral and momentum responses, resulting in broadband impedance matching for waveguides coupling to high-quality-factor deformed resonators[46]. Notably, this result allows one to overcome the traditional bandwidth limitation in evanescent coupling methods.

Because of the difficulty in clarifying the relationship between the deformation and chaotic phenomena, most approaches have focused on controlling a few scalar parameters[46,56,57] that manipulate the boundary of microdisks. Further design freedom should be enabled by microdisks composed of inhomogeneous media or by the introduction of multiple parameters for the sophisticated design of microdisk boundaries. For example, transformation optics enables the deterministic deformation of microdisks made of inhomogeneous metamaterials with unidirectional emission[59].

Engineered hyperuniform structures with complete photonic bandgaps. The concept of disordered hyperuniformity[4] has dramatically changed our understanding of the nature of randomness and order and, hence, provides new challenges for the development of sensitive order metrics. Because all perfect crystals and quasicrystals are hyperuniform[4,41,60], hyperuniformity provides a unified framework to structurally characterize and categorize — via hyperuniformity order metrics[4,41,60] or τ order metrics[40] — crystals, quasicrystals and their exotic disordered varieties. The latter are ideal amorphous states of matter that lie between a crystal and a liquid: they are like perfect crystals in the way they suppress large-scale density fluctuations (BOX 1), a special type of long-range order, and, yet, are like liquids or glasses in that they are statistically isotropic with no Bragg peaks and, hence, lack any conventional long-range order[60]. The fact that such exotic amorphous states of matter have characteristics of both conventional crystals and disordered systems endows them with novel thermodynamic[40,61] and physical properties[5,47,60,62].

Disordered hyperuniformity is, therefore, an illustrative example of engineered disorder for controlling both spectral (PBGs) and momentum (directivity) responses of light. This concept led to a breakthrough in PBG research, enabling the first disordered dielectric networks with complete PBGs that were perfectly isotropic and comparable in size to those in photonic crystals[47] (TABLE 1). In particular, stealthy hyperuniform patterns[40,50] were used, in which the structure factor $S(\mathbf{k})$ was zero for all wavenumbers $k < K$ (BOX 1). FIGURE 4a shows the difference between a stealthy hyperuniform pattern and a non-hyperuniform pattern. Disordered stealthy hyperuniform materials enable free-form waveguides with novel geometries not possible with photonic crystals[5].

An outstanding theoretical question is whether finite-sized PBGs in disordered designs persist in the infinite-sample-size limit and what are the required structural conditions to ensure they do. It was argued that, to achieve large PBGs that do not vanish in the large-sample limit, stealthy hyperuniformity, combined with uniform local topology and short-range geometric order, was necessary[47]. The importance of short-range order and hyperuniformity (rather than stealthiness) was also suggested for the formation of complete PBGs[63], but relatively small systems (200 particles) were considered. Recently, it was conjectured that the 'bounded-hole' property of stealthy hyperuniform systems — which avoid the emergence of a large-sized region empty of particle centres — is crucial for complete PBGs in the infinite-system-size limit[60], which is related to the increase in short-range order as the stealthiness increases. Following these theoretical results, stealthy hyperuniform patterns have enabled the systematic generation of complete PBGs in disordered materials (FIG. 4b) and other types of spectral engineering, including superior robustness and isotropy of stealthy hyperuniform PBGs at short wavelength[5] and full transparency to light resistant to multiple scattering at long wavelengths[62]. Practical implementations of hyperuniform systems have been realized, mostly using top-down fabrication, such as direct laser writing and atomic layer deposition[64], and, for microwave samples, stereolithography[5] (FIG. 4b). Bottom-up fabrication of hyperuniform or stealthy hyperuniform structures has also been achieved using 3D printing for fibres[65] and self-stabilized colloid deposition[66].

Disordered families for isospectrality. Another route to achieving order-like spectral properties in disordered structures has been inspired by the classic question: "Can one hear the shape of a drum?"[67]. The sound of a drum is the linear combination of the tones allowed by the elastic membrane potential (its eigenvalues). To hear the shape of a drum, there should be a one-to-one correspondence between the potential landscape and a

Box 2 | **The concept of order metrics**

To focus on the basic issues concerning order metrics, we restrict the discussion to systems consisting of N particles in the d-dimensional Euclidean space R^d. Such many-body systems are characterized statistically by their N-body probability density function $P_N(\mathbf{R})$, which is the probability of finding the N-particle system with configuration $\mathbf{R}$ (dN-dimensional coordinate). Such complete information is virtually never available for large N and, in practice, one must settle for reduced information, such as a scalar order metric ψ. A good order metric $\psi(\mathbf{R})$ should have the following properties: be a well-defined function sensitive to any type of ordering, without bias towards any reference system; provide the hierarchy of ordering between prototypical systems given by common physical intuition (for example, crystals, followed by quasicrystals, defective crystals and quasicrystals, correlated disorder without long-range order and, finally, uncorrelated disorder), so that, for any two configurations $\mathbf{R}_A$ and $\mathbf{R}_B$, $\psi(\mathbf{R}_A) > \psi(\mathbf{R}_B)$ implies that configuration $\mathbf{R}_A$ is to be considered as more ordered than configuration $\mathbf{R}_B$; incorporate both the variety of local coordination patterns and the spatial distribution of such patterns; satisfy the normalization condition $0 \leq \psi \leq 1$ (where zero and unity indicate the least and most ordered system, respectively); and be able to detect translational and orientational order at any length scale. One can construct a useful set of order metrics $\psi_1, \psi_2, \psi_3 \ldots$ that are positively correlated with one another and, hence, lead to consistent results in classifying disorder.

Table 1 | **Examples of engineered disorder**

Phenomena controlled by disorder	Physics	Order metric (OM) or design parameter (DP) of the degree of disorder	Target quantities	
			Order	Uncorrelated disorder
Spectral response	Dynamical tunnelling to chaotic channels[46]	Perturbation ε of the microdisk radius (OM)	High-*Q*-factor resonances	Broad impedance matching
	Stealthy hyperuniformity for PBG materials[5]	τ or hyperuniformity order metrics (OM)	Complete TE and TM PBGs	Isotropic PBGs
	Isospectrality using SUSY transformation[42]	Hurst exponent *H* for long-range correlation (OM)	PBGs without defect states	Short localization length
Localization/ transport	Enhanced localization at sub-λ using the GH shift[96]	λ-normalized interval of a uniform distribution (OM)	Homogeneous effective permittivity	Angle-specific short localization length
	Phase-conserved energy confinement[108]	Perturbation in the spatial amplitude (OM)	Plane-wave-like spatial phase	Spatially localized optical energy
Wavefront/ directivity	Wavefront shaping using disordered metasurfaces[127]	Target angular range for spatial phase function (DP)	Large optical memory effect	Large scattering angle
	Reflectors mimicking *Morpho* butterfly wings[133]	Distribution of microsphere diameters (DP)	Narrowband reflection spectra	Broadband angular responses
Topology/ spin–orbit	Photonic topological Anderson insulators[137]	On-site disorder with uniform randomness (OM)	Topological edge states for transport	Localized bulk states

The table lists selected works on the underlying physics, order metrics and target wave quantities ($Q_{p,q}$ in the text and in FIG. 2) of disordered systems. For studies in which an order metric was not explicitly defined, the key design parameter that determines the degree of disorder is listed. GH, Goos–Hänchen; PBG, photonic bandgap; *Q*-factor, quality factor; SUSY, supersymmetry; TE, transverse electric; TM, transverse magnetic; λ, wavelength.

set of eigenvalues. It has been demonstrated that this is not the case[68], as there is a one-to-many correspondence between a set of eigenvalues and the potential landscapes that can generate them: there is isospectrality between different potentials.

Various physical symmetries, such as translational, rotational and chiral symmetries, provide a straightforward set of isospectral potentials yet preserve the order metrics of the original potentials. However, some non-trivial symmetries resulting in perfect isospectrality or quasi-isospectrality open up the possibility of tuning disorder while maintaining the spectral response, even allowing isospectral relations between ordered and highly disordered structures.

Isospectrality with controlled disorder can be realized in photonics by the supersymmetry (SUSY) transformation[69]. The SUSY transformation is mathematically based on the Darboux factorization of the Hamiltonian *H*, which applies to 1D potential landscapes. The factorization decomposes the Hamiltonian as $H = BA$, where *A* and *B* are partial operators with lower-order derivatives than that of *H*. The application of the partial operator *A* to the eigenvalue equation $H\psi_n = E_n\psi_n$ transforms the original Hamiltonian *H* to a new SUSY Hamiltonian $H_s = AB$, which has a potential landscape with a deformed profile and preserves the original eigenvalues E_n, except for that of the ground state, E_0 (FIG. 5a). This quasi-isospectral deformation, which satisfies global phase matching with the selective annihilation of an eigenmode, has been applied to mode-division multiplexing[70] and to the stable emission of a fundamental lasing mode[71].

The deformation of the potential landscapes in the SUSY transformation fulfils the condition of nontrivial isospectrality. Starting from the seed potentials of crystals and quasicrystals, the successive application of SUSY transformations enables the deterministic control of the long-range autocorrelation of disordered potential landscapes while preserving crystal-like spectra[42]. When the Hurst exponent *H* is used as the order metric (TABLE 1) — $0 \le H \le 0.5$ for negative correlations and $0.5 \le H \le 1$ for positive correlations — a series of SUSY transformations allows the design of different disordered potentials with controlled correlations ($0 \le H \le 0.8$) for the same PBG[42]. This transformation of order to isospectrally engineered disorder enables the independent control of wave characteristics in disordered structures, enabling PBG structures with tunable levels of disorder (FIG. 5b), a disorder-induced change in the localization length[42] (FIG. 5a and TABLE 1) and disordered Wannier–Stark ladder potentials for stable Bloch oscillation[72,73] (FIG. 5c). Although the SUSY-induced deformation of potential landscapes generally occurs regardless of the size of the potential, most research efforts have focused on the modification of spatially localized potentials or arrays, including studies on complex-valued disordered potentials with real-valued eigenspectra[74] and on the identical scattering between a metal–dielectric grating and a SUSY-deformed dielectric grating[75]. Further studies examining the order metric over various types of large-scale SUSY-transformed potentials are necessary to precisely control target wave properties while preserving the spectral response.

The SUSY transformation is a powerful tool that enables the solvable handling of arbitrary potential landscapes. However, the difficulty in factorizing multi-dimensional Hamiltonians restricts the application of SUSY to 1D problems, although this limit has been partially resolved through the separation of variables[42] or the combination of SUSY-transformed potentials[76].

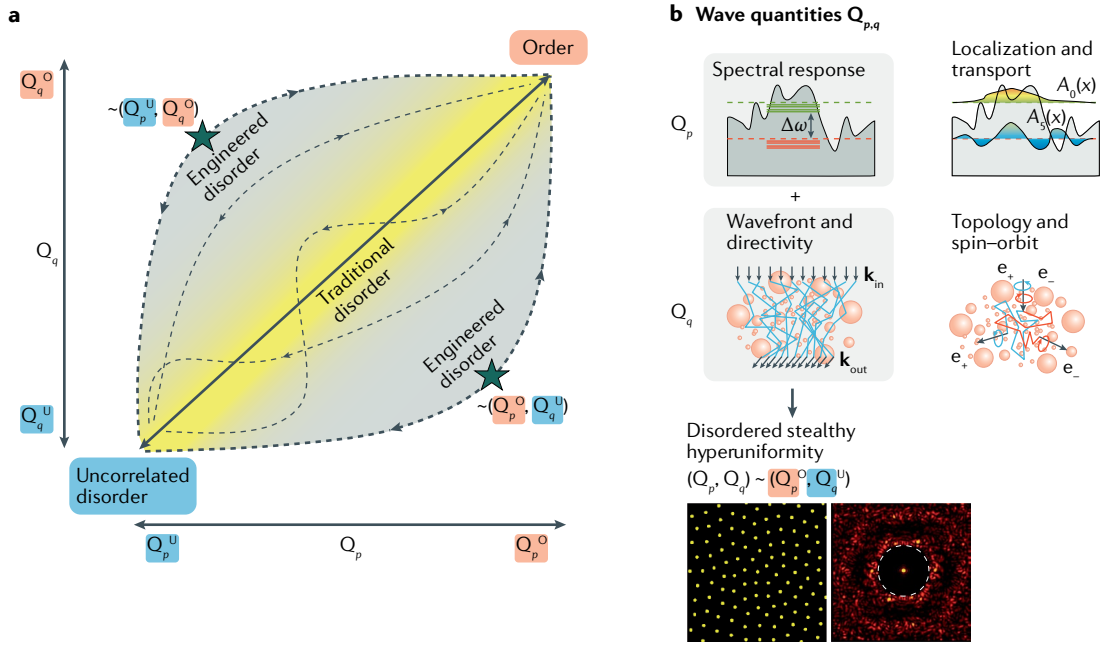

Fig. 2 | **Engineering disorder by designing nontrivial loci between order and uncorrelated disorder. a** | The concept of engineered disorder. The Q_p and Q_q axes represent the state of each of two target wave quantities, spanning from an ordered state (Q_p^O and Q_q^O) to a state of uncorrelated disorder (Q_p^U and Q_q^U). A trivial transition (coloured line and yellow region) results in the gradual changes $Q_p^O \rightarrow Q_p^U$ and $Q_q^O \rightarrow Q_q^U$. Engineering disorder gives access to more extended regimes (grey regions and dashed lines) achieving the coexistence of properties typical of order and uncorrelated disorder (as in the points highlighted by the stars). **b** | An example of engineered disorder, in this case, designed to manipulate the spectral response (Q_p) and directivity (Q_q). This engineered disorder can be used to obtain order-like spectral responses and uncorrelated-disorder-like directivity, as $(Q_p, Q_q) \sim (Q_p^O, Q_q^U)$. Disordered stealthy hyperuniform materials are one example of such engineered disordered structures, which leads to a crystal-like photonic bandgap and uncorrelated-disorder-like isotropy. $\Delta\omega$, photonic bandgap; $A_0(x)$ and $A_5(x)$, spatial profiles of the 0th and 5th eigenmodes, respectively; $\mathbf{k}_{in}$ and $\mathbf{k}_{out}$, input and output wavevectors, respectively; $\mathbf{e}_{\pm}$, spin components.

In the context of dimensionality, the Householder[77,78] or Lanczos[79] transformations have been studied for the isospectrality between structures with different dimensionalities. Both transformations isospectrally remove far-off electromagnetic couplings for disordered optical structures, which enables the dimensional reduction to 1D structures while preserving the spectral properties. Lossless signal transport between structures with different dimensionality[77] (FIG. 5d) and single-mode operation in a disordered laser array[78] were demonstrated using the Householder transformation. Recently, the excitation dynamics of localization in a disordered 7D hypercube lattice was achieved in a 1D structure using the Lanczos transformation[79].

Engineered localization and transport

Periodic systems with discrete translational symmetry conserve the Bloch momentum of waves, leading to ballistic wave transport. By contrast, disordered structures with partially or entirely broken translational symmetry alter the Bloch momentum state, usually degrading the transport efficiency and, eventually, resulting in wave diffusion or localization. Such disorder-induced changes are ubiquitous in liquids and glasses, and are at the base of the white colour of milk, fog and teeth.

In 1958, Phillip Anderson first demonstrated that a complete halt of wave transport is achieved with strong disorder, owing to a phenomenon now known as Anderson localization[14]. When analysing localization in general, the dimensionality of a system plays a critical role, as described by the scaling theory of localization[80]. A localized system is characterized by a specific length scale beyond which the state exhibits substantially suppressed electron (or photon) mobility. This length scale is described by the scaling function $\beta(g)$ (FIG. 6a), which represents the variation of the electronic conductance (or of the photon-transport efficiency), $g(L)$, where L is the size of the system. Under the assumption that the material is homogeneous and isotropic with elastic scattering[81] (FIG. 6b), the well-known conductance of a macroscopic ohmic conductor (for large g) or insulator (for small g) leads to the asymptotic behaviour of $\beta(g)$. Notably, only 3D systems can provide extended states, offering a metal–insulator transition across $\beta(g) = 0$. Every 1D or 2D system eventually results in localization, though the localization length can be controlled according to the system configuration.

Because photonic systems do not allow interactions between waves and can accommodate time-invariant potentials, photonic structures provide attractive platforms for the observation of localization[82]. By exploiting the mathematical analogy between the scalar form of the time-independent Maxwell's equations and the time-dependent Schrödinger equation, the concept of transverse Anderson localization of light was theoretically proposed[83]. After a landmark observation of

microwave localization in a quasi-1D geometry[84], weak or strong transverse localization has been experimentally demonstrated in various 1D[85,86] or 2D[87,88] photonic systems, in which even negligible scattering produces transverse localization. Among the unresolved issues is the experimental observation of Anderson localization in 3D structures, which is hindered by multiple factors, including insufficient material contrast, near-field effects and the effects of absorption[89].

In this section, we discuss recent achievements in engineered disorder in terms of wave localization, focusing on two topics: engineered transverse localization by utilizing subwavelength disorder and engineered diffusion or transport beyond the assumptions[81] of the scaling theory of localization.

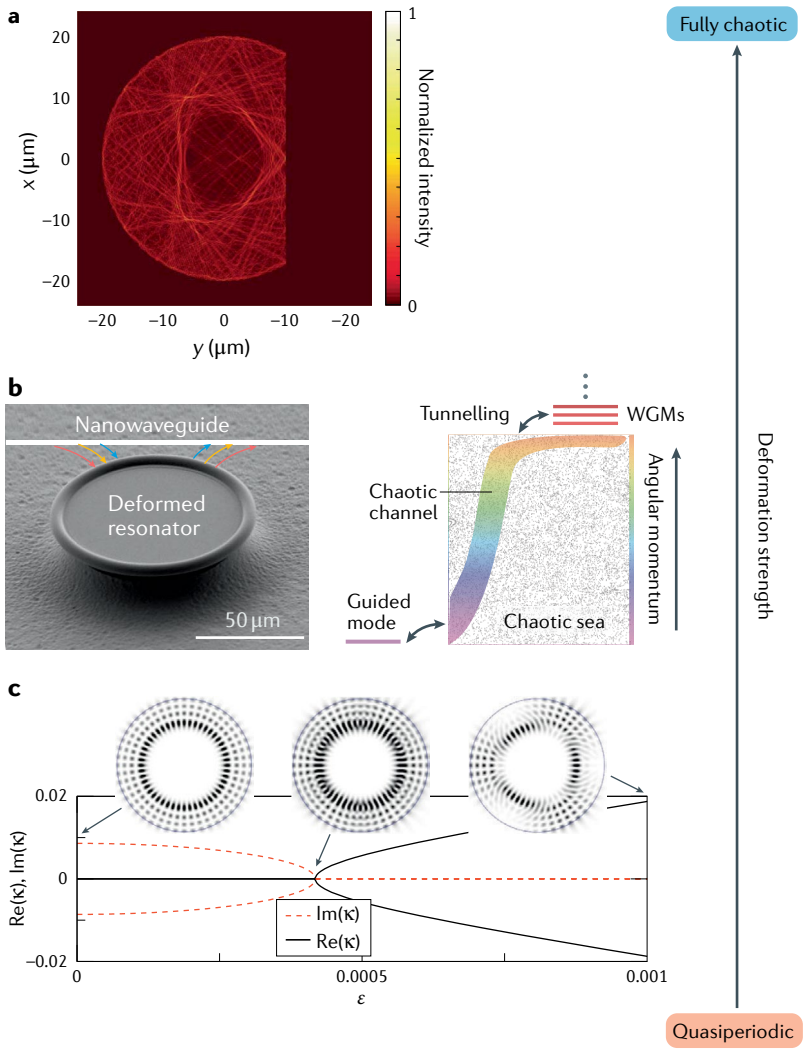

Fig. 3 | **Engineered spectral responses in deformed microcavities. a** | Chaotic intensity distribution of a high-quality-factor mode in a strongly deformed (D-shaped) dielectric cavity. The strong deformation prohibits the build-up of coherent waves, leading to the spatiotemporal stabilization of a laser with suppressed nonlinear modal interactions[56]. **b** | Broadband coupling to a high-quality-factor resonator (left) through a dynamic tunnelling process (right): the coupling between whispering gallery modes (WGMs) and guided modes happens through chaotic channels in phase space[46]. **c** | Exceptional points derived by extremely weak deformation (ε) of a cavity[57]. The cavity is defined by the limaçon-type deformation of its radius $r(\varphi) = R[1 + \varepsilon\cos(3\varphi)]$ along the azimuthal axis φ. An exceptional point emerges at $\varepsilon \sim 4 \times 10^{-4}$, where the real (Re) and imaginary (Im) parts of the eigenvalues κ coalesce, and can be exploited for the design of very sensitive photonic devices. Panel **a** reprinted with permission from REF.[56], AAAS. Panel **b** reprinted with permission from REF.[46], AAAS. Panel **c** is adapted with permission from REF.[57], APS.

Transverse localization in subwavelength platforms. Localization arises from the interference between scattered waves. Studies on localization have, thus, focused on features of size comparable to or larger than the wavelength λ, because subwavelength disorder causes negligible scattering with very long localization length (very large g in FIG. 6a). However, precision nanofabrication techniques allow achieving of enhanced interference with carefully arranged subwavelength structures composing scattering centres that substantially reduce the localization length (green and blue arrows in FIG. 6a).

One instructive example of well-arranged subwavelength disorder for transverse localization in 2D can be found in nature: protein nanostructures in native silk produced by silkworms (*Bombyx mori*)[90]. A silk fibroin filament contains ~3,800 nanofibrils with a size of ~25 nm (FIG. 6c). Individual fibrils cannot serve as a scattering centre. However, owing to their statistical distributions and volume fractions, nanofibrils form clusters that provide substantial scattering for λ = ~600 nm. Native silk, thus, exhibits transverse Anderson localization in the visible and near-infrared regions, in contrast to conventional biological media, usually exhibiting diffusion or very large localization lengths. Because Anderson localization induces enhanced reflectivity in the corresponding spectra, native silk with high emissivity in the infrared region can be used for passive radiative cooling. A similar transverse Anderson localization has been demonstrated in artificial fibres[91,92] to realize focusing inside the fibre and single-mode transmission. The arrangement of subwavelength structures has also been studied in nanophotonic waveguide networks, achieving mirrorless lasing arising from localization and controlled by network connectivity[93].

Although the examples above[90–93] utilize subwavelength elements, the resulting scattering centres have features of size comparable to (or larger than) λ, forming inhomogeneous distributions of effective material parameters at the ~λ scale according to effective medium theories, such as the Maxwell–Garnett theory[94]. By contrast, for an effectively homogeneous material, it was believed that one cannot experimentally observe localization due to a very large localization length and the finite size of a sample, even when the medium is highly disordered at the deep-subwavelength scale.

Recent studies on the failure of the effective medium theory[95] have initiated the breaking of this traditional length-scale limitation in 1D geometries, achieving measurable transverse Anderson localization in deeply subwavelength structures (or homogeneous effective media)[96]. Classical studies on Anderson localization considered the scattering of propagating waves, which accumulate phase through propagation. By contrast, evanescent waves do not accumulate phase through propagation, but they accumulate phase upon scattering at the interface between different media through the Goos–Hänchen (GH) phase shift. Unlike the

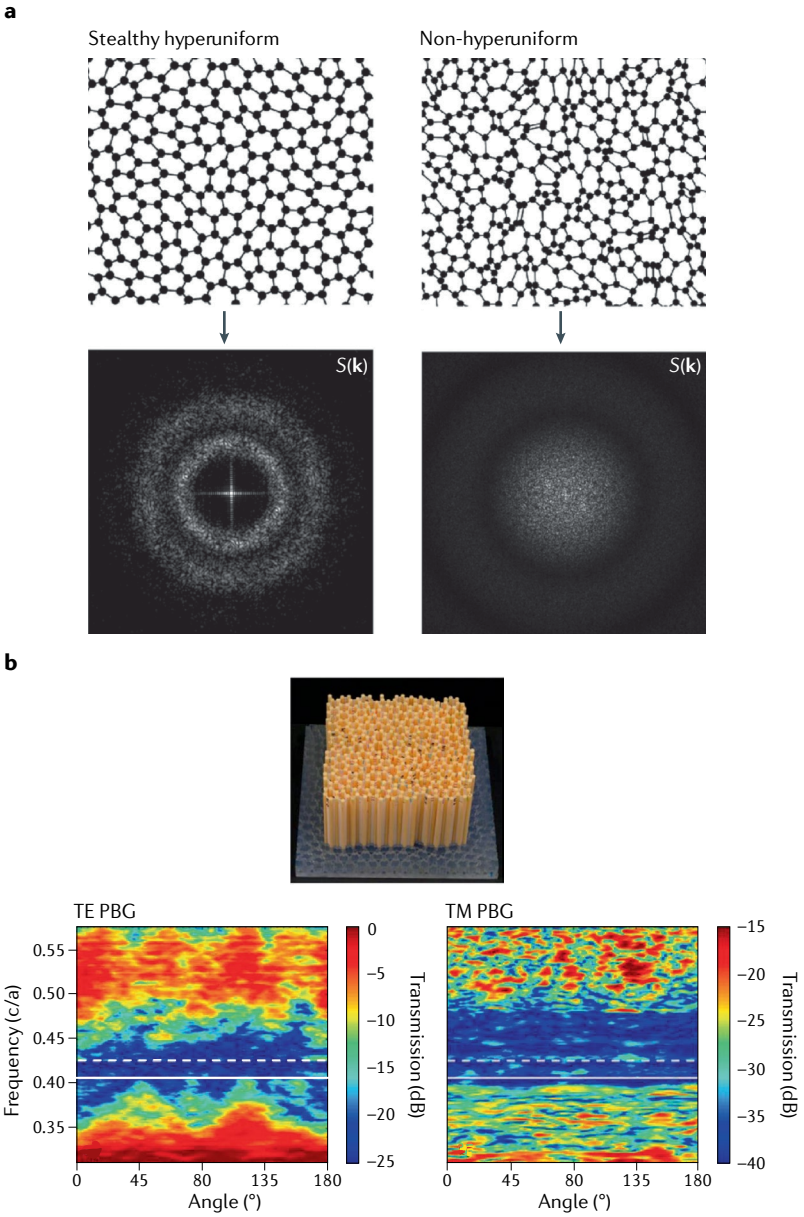

Fig. 4 | **Engineered spectral responses in hyperuniform structures. a** | A comparison between a stealthy hyperuniform and a non-hyperuniform pattern[47], along with their corresponding $S(\mathbf{k})$. The stealthy hyperuniform pattern shows the suppression of the structure factor $S(\mathbf{k})$ for $|\mathbf{k}| < K$. **b** | Isotropic complete bandgaps in a 2D stealthy hyperuniform structure[5] for both transverse-electric (TE) and transverse-magnetic (TM) modes. PBG, photonic bandgap. Panel **a** reprinted with permission from REF.[47], PNAS. Panel **b** reprinted with permission from REF.[5], PNAS.

distance-dependent phase accumulation of propagating waves, the phase accumulation through the GH shift occurs immediately at the material interface, without needing the propagation length for the phase accumulation. This immediate phase accumulation leads to the breakdown of the effective medium theory[95] and to the emergence of 'interface-type' scattering centres in producing sufficiently strong random scattering (or small g in FIG. 6a) for the observation of transverse Anderson localization at the deep-subwavelength scale (FIG. 6d). Because the GH shift is dependent on the incident angle, the deeply subwavelength disorder needed to realize Anderson localization in this case has a strong angle dependency, whereas the effective parameters of the system are those of a homogeneous medium. Disorder engineered using the GH shift, therefore, enables the independent control of the effective medium theory parameters and of the localization length, which depends on the incident angle (TABLE 1). This phenomenon was experimentally demonstrated[97] by observing disorder-induced reflection changes in layers with a thickness of ~λ/40: a 2-nm structural modification could be sensed with localized visible light.

Engineered transport in inhomogeneous or non-Hermitian systems. The scaling theory[80] predicts that all states in 1D or 2D disordered systems are eventually localized when the systems satisfy the conditions of homogeneity, isotropy and elastic scattering[81] (FIG. 6b). By alleviating these conditions, extended states and delocalization can be realized even in 1D or 2D disordered systems, as shown in studies on electronic delocalization in inhomogeneous[98] or anisotropic[99] systems. Alleviating the condition of elastic scattering implies entering the regime of non-Hermitian photonics[100], which exploits complex-valued potentials with gain or loss for controlling light behaviours. Here, we focus on inhomogeneous and non-Hermitian systems to manipulate the diffusion or transport of light. These distinct transport behaviours can be quantified using the diffusion exponent α, which is related to the increase of the average squared displacement of light with time or space as $\langle x^2 \rangle \sim t^{\alpha}$, where $\alpha = 2$ for ballistic transport, $\alpha = 1$ for normal diffusion and $\alpha = 0$ for localization.

A typical example of an inhomogeneous material is a Lévy glass[101], which is the structural realization of the Lévy flight: a random walk in which the step lengths have a heavy-tailed, power-law probability distribution. The spatial inhomogeneity of scatterer density in a Lévy glass follows the probability distribution of the Lévy flight. This Lévy-flight scatterer density was practically realized using glass microspheres with a diameter d following the power-law distribution $P_s(d) \sim d^{-\delta}$ (with δ the order metric) placed inside a glass matrix with a controlled spatial density of high-index (titanium-dioxide) nanoparticles. This Lévy glass has a scale-invariant structure, with elements connected by clusters of short steps and frequent long steps (FIG. 6e, left), analogous to the hub connections in scale-free networks[2]. Similar to the enhanced transport in scale-free networks[2], superdiffusive light transport ($1 < \alpha < 2$) has been achieved in Lévy glasses[102,103] with order metric $\delta \sim 3$, which exhibit more strongly fluctuating transmission profiles than normal diffusive structures (FIG. 6e, right). In this context, the relationship between a Lévy glass and a system with uncorrelated disorder is analogous to that between a scale-free and random graph in network theory. This viewpoint should inspire further study in disordered photonics towards the realization of photonic structures analogous to complex graph networks.

Lévy glasses and other types of systems with correlated disorder[104] have enabled significant changes in wave behaviour in a given transport regime, including tuning the diffusion efficiency ($\alpha \sim 1$) and localization

length ($\alpha \sim 0$). The phase transition between transparent ($\alpha = 2$) and opaque ($\alpha = 0$) media, as the metal–insulator transition in condensed-matter physics, is only allowed in 3D systems. However, it would be interesting to obtain it also in 1D and 2D systems. In recent works, instead of altering all the eigenmodes of a disordered structure for a complete phase transition, the deterministic control of a partial set of eigenmodes has been exploited for practical applications. One representative example is non-Hermitian photonics[100] with non-conserved energy, which corresponds to the breaking of the elastic scattering condition in the scaling theory[81]. For example, constant-intensity wave transport[105–109] and phase-conserved energy confinement[108] (FIG. 6f) have been realized in disordered complex potentials. Such potentials are inversely designed starting from the prescribed target eigenmode. Therefore, an order metric in these works is indirectly defined by the degree of disorder in the target eigenmode: the perturbation in the phase function for the constant-intensity transport and the perturbation in the amplitude function for the phase-conserved energy confinement (TABLE 1). These intriguing wave behaviours can be understood in the context of the Bohmian formulation of quantum phenomena, realizing the independent control of the phase and amplitude of light in complex-valued optical potentials[108], which is the main feature of engineered disorder. Similar approaches for designed eigenmodes in disordered structures have also been studied in Hermitian systems with the combination of diagonal and off-diagonal disorder[106]. Although the engineering of a partial set of eigenmodes has been applied to overcome instabilities in lasers[107] and to realize perfect transport (~100%) inside disordered structures[106–108], there is a critical restriction on the initial condition: only a fixed incident angle and frequency achieve the designed wave transport. One direction for future research is, then, to design the collective delocalization of multiple eigenmodes, as observed in the Hatano–Nelson model[110].

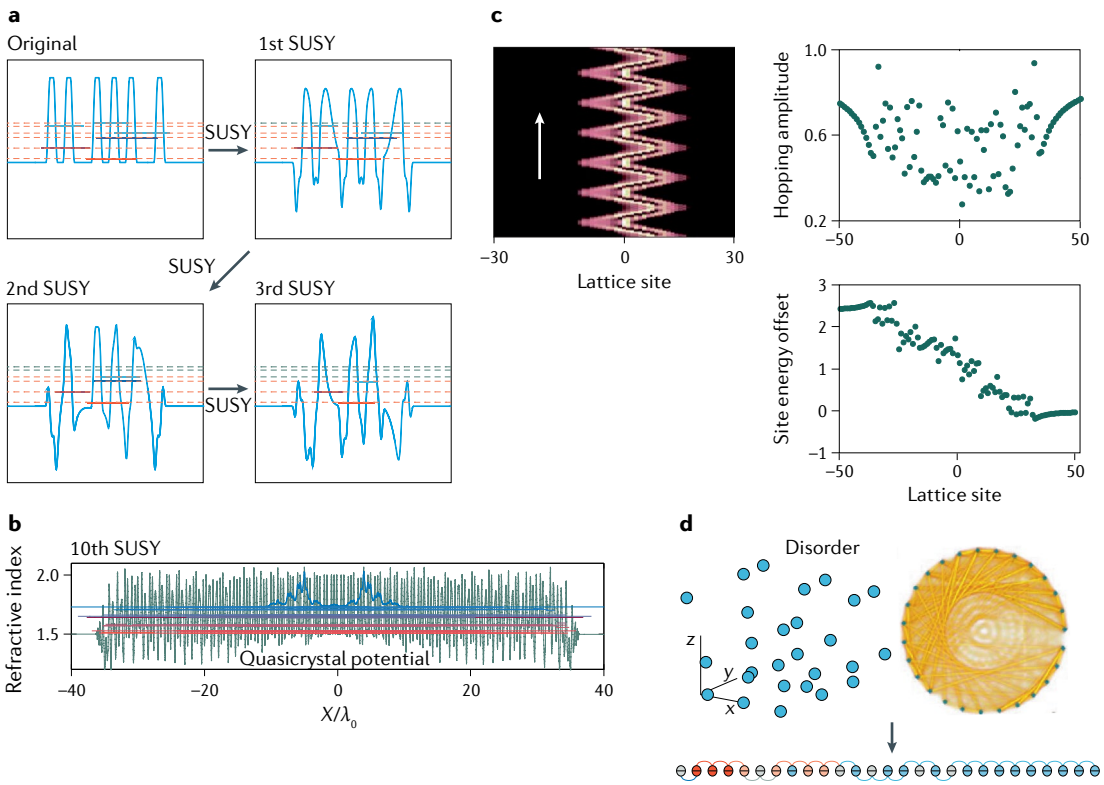

Fig. 5 | **Engineered spectral responses using isospectrality. a** | Quasi-isospectral deformation of an optical potential achieved by successive supersymmetry (SUSY) transformations. The landscapes describe the refractive index profiles at each step. The orange dashed lines represent the preserved eigenmodes, the green dashed lines the annihilated eigenmodes. **b** | SUSY-deformed quasicrystal with a photonic bandgap[42]. The potential (green line) is obtained by applying ten successive SUSY transformations to a 1D Fibonacci quasicrystal. The blue curve represents the spatial profile of the ground state. The horizontal lengths and vertical positions of the coloured lines in panels **a** and **b** represent the spatial and spectral distributions of the eigenmodes, respectively. λ_0, free-space wavelength. **c** | Bloch oscillation in a disordered Wannier–Stark ladder. The hopping amplitude and site energy offset in the potential are shown on the right side of the panel[72]. The potential is obtained by applying 12 successive SUSY transformations to the perfect Wannier–Stark ladder. The arrow represents the propagation direction. **d** | Isospectrality between structures with different dimensionality can be obtained using the Householder transformation of graph networks[77]: the initial 3D structure, its graph representation and the 1D isospectral design are shown in this panel. In the 1D structure, the colours of the spheres and their connecting curves represent the values of the resonance modification of each element and the coupling between them, respectively. Panels **a** and **b** are adapted from REF.[42], CC BY 4.0 (https://creativecommons/org/licenses/by/4.0/). Panel **c** reprinted with permission from REF.[72], APS. Panel **d** is adapted with permission from REF.[77], © The Optical Society.

Engineered wavefront and directivity

The controlled directivity and wavefront of scattered light determine optical functions in the far-field regime. Traditional approaches for controlling the directivity have primarily employed ordered structures, such as Bragg gratings[7], photonic crystals[8] and, more recently, metasurfaces[111], and are based on the independent manipulation of each diffraction order of scattered light to achieve far-field functionalities.

By contrast, most natural structures have complex and turbid material configurations with inhomogeneous refractive index. The deterministic design of the metric is defined by the ratio between the uniform distribution interval (16 nm) and the optical wavelength. For oblique incidence (~60°), the Goos–Hänchen shift plays an important role, as it induces phase accumulation and localization, despite the deep-subwavelength length scales: the layer is, on average, 10 nm thick, whereas the wavelength is 10 μm. **e** | Lévy flight in an inhomogeneous medium. Left: red lines for Monte-Carlo-simulated random-walker trajectory show the frequent emergence of long steps. The magnification in the inset shows the scale invariance of the structure. Right: spatial distributions of the transmitted intensity obtained from two different realizations of disorder for a Lévy glass (top) and for a normal diffusive sample (bottom). Although a normal diffusive sample results in nearly constant spatial distributions, a Lévy glass exhibits a large difference between different realizations. **f** | A disordered, complex-valued optical structure that achieves phase-conserved energy confinement[108]. Panel **c** reprinted from REF.[90], CC BY 4.0 (https://creativecommons.org/licenses/by/4.0/). Panel **d** reprinted from REF.[96], CC BY 4.0 (https://creativecommons.org/licenses/by/4.0/). Panel **e** adapted from REF.[101], Springer Nature Limited. Panel **f** reprinted from REF.[108], CC BY 4.0 (https://creativecommons.org/licenses/by/4.0/).

directivity and wavefront of light interacting with disordered structures is, thus, challenging, especially for biomedical applications, such as the focusing of electromagnetic energy on a target location inside the human body[112]. The most common approach consists in using wavefront-shaping techniques[113,114], which are based on the optimization of the impinging wavefront to achieve designed constructive interference at a target position. Disordered structures in nature have also inspired the engineering of functional far-field phenomena, such as structural colours[20], omnidirectional antireflection[115] and perfect absorption[116]. This section introduces recent achievements, focusing particularly on engineered disorder for wavefront shaping and engineered disorder inspired by biological structures.

Engineered disorder for wavefront shaping. Biological structures are naturally disordered media. Although scattering inside static and lossless media does not result in an irreversible loss of information[117], the coherence, directivity and focusing of incident light are usually destroyed, hindering functional responses inside turbid media. After the first realization of designed focusing through disordered media[113] and its generalization through the measurement of the transmission matrix[114], a wavefront-shaping technique[113,114,118] has been developed that modifies the spatial profile of light with a spatial light modulator (SLM) to achieve optical functionalities through or within disordered structures. This technique has been extended to include the utilization of spatiotemporal degrees of freedom[112] and guidestar-assisted methods[119] for biomedical applications, including optogenetic neuron controls and deep-tissue imaging. The theoretical background underpinning wavefront shaping based on mesoscopic-scattering theory was rigorously described in the review article in REF.[120].

Owing to the mechanism underlying wavefront shaping — interactions between modulated light and disordered matter — the engineering of disorder has been sought in two ways: engineering the modulated light or the disordered structures. In analogy to anomalously large conductance fluctuations of electron transport in systems with mesoscopic structural correlations[121], the effect of long-range correlations in the wavefront-shaping transmission matrix was investigated for targets larger than a single speckle[122]. In examples of target focusing or defocusing through disordered media (FIG. 7a), the range of control on the total transmitted flux into the focal target is substantially enhanced by using SLM-modulated light. This enhancement originates from the long-range correlation between transmission-matrix elements, which is obtained from the optimized 'wavefront' (or engineered disorder in light, FIG. 7b).

Wavefront shaping has also been used in disordered 'platforms' to enhance optical functionalities, for example, to make lenses with high numerical aperture (NA). In line with results in ultrasound[123] and microwave[124] platforms, disordered structures have been exploited[118,125,126] to increase the NA in light focusing, obtaining a resolution 5–10 times better than the diffraction limit[118,125], enabling sub-100-nm resolution with visible light[126].

Building upon these results in systems with randomly assigned disorder[118,123–126], engineered disorder was recently introduced through disorder-engineered metasurfaces[127] (FIG. 7c), which break the limitation in spatial frequencies that, in an SLM, is imposed by the pixel pitch, d. Indeed, these metasurfaces give access to much higher spatial frequencies than those afforded by conventional SLM methods, as $\nu \leq (1/\lambda)$, in contrast to the SLM limit $\nu \leq 1/(2d)$ (usually, $d >> 10\lambda$). The higher frequencies allow for an increase in the number of addressable focal spots. These disorder-engineered metasurfaces were designed through the optimization of the spatial phase function using the Gerchberg–Saxton algorithm, to yield an isotropic scattering profile over the target angular range. Although a specific order metric was not estimated for the metasurfaces, their degree of disorder was determined by the target angular range (TABLE 1).

Disorder-engineered metasurfaces[127] also display a superior optical memory effect (FIG. 7d). This effect arises from the scattering-based correlation between the changes in the input and output wavefront, allowing for the manipulation of the output wavefront with the modulated input. Although this correlation is usually separated in a 'tilt' (REF.[128]) and a 'shift' (REF.[129]) function for the momentum and spatial perturbation of light, respectively, recent work[130] proved that these two components are interrelated. In conventional 3D disordered media, it is difficult to achieve a large memory effect with a wide angular scattering range, because a thick sample has a wide angular profile[130], which results in a decreased memory effect. By contrast, a disorder-engineered metasurface[127], whose meta-atoms have resonances with low angular sensitivity, results in an angular correlation (or memory effect) range of ~30°, much more extensive than that of conventional disordered media (<5°), while maintaining a large scattering angle (~90°). This results in a high NA and stable focusing that can be used for imaging in biomedical applications (FIG. 7c).

Biomimetic engineering. The effort to engineer disordered systems to mimic biological structures has provided insight into the control of far-field functionalities of light, in particular, for the reproduction of structural colours, such as those produced by photonic nanostructures with short-range order found in the feathers of birds[20]. For example, it was revealed that the white colour of white beetles originates from the network morphology of the wing scales[131]. The intriguing role of disorder in floral-grating-like structures, such as the angiosperm *Hibiscus trionum*, was also studied[132], demonstrating that the generation of visual signals from angle-dependent scattering at striated flower surfaces (FIG. 7e, top) strongly depends on the level of disorder at the length scales corresponding to ultraviolet and blue wavelengths. The resulting iridescent optical signals are noticeable to bees, proving the role of structural disorder in biological functions. 'Artificial flowers' made of nanoscale grating structures (FIG. 7e, bottom) were created based on engineered disorder and shown to produce a photonic signature that is highly attractive to insect pollinators.

The *Morpho didius* butterfly is another example of the use of functional disorder in nature. It displays

both a vivid blue colour and wide angular reflections. The coexistence of crystal-like narrowband spectral information and disorder-like broadband angular responses originates from the structural combination of order and disorder[133] (FIG. 7f, left), embodied in the quasiperiodicity of the multilayers in a unit cell and their in-plane random distribution. This structural configuration was reproduced in silicon-based nanophotonic platforms (FIG. 7f, right and bottom)[133], with alternating silicon-dioxide and titanium-dioxide layers on a

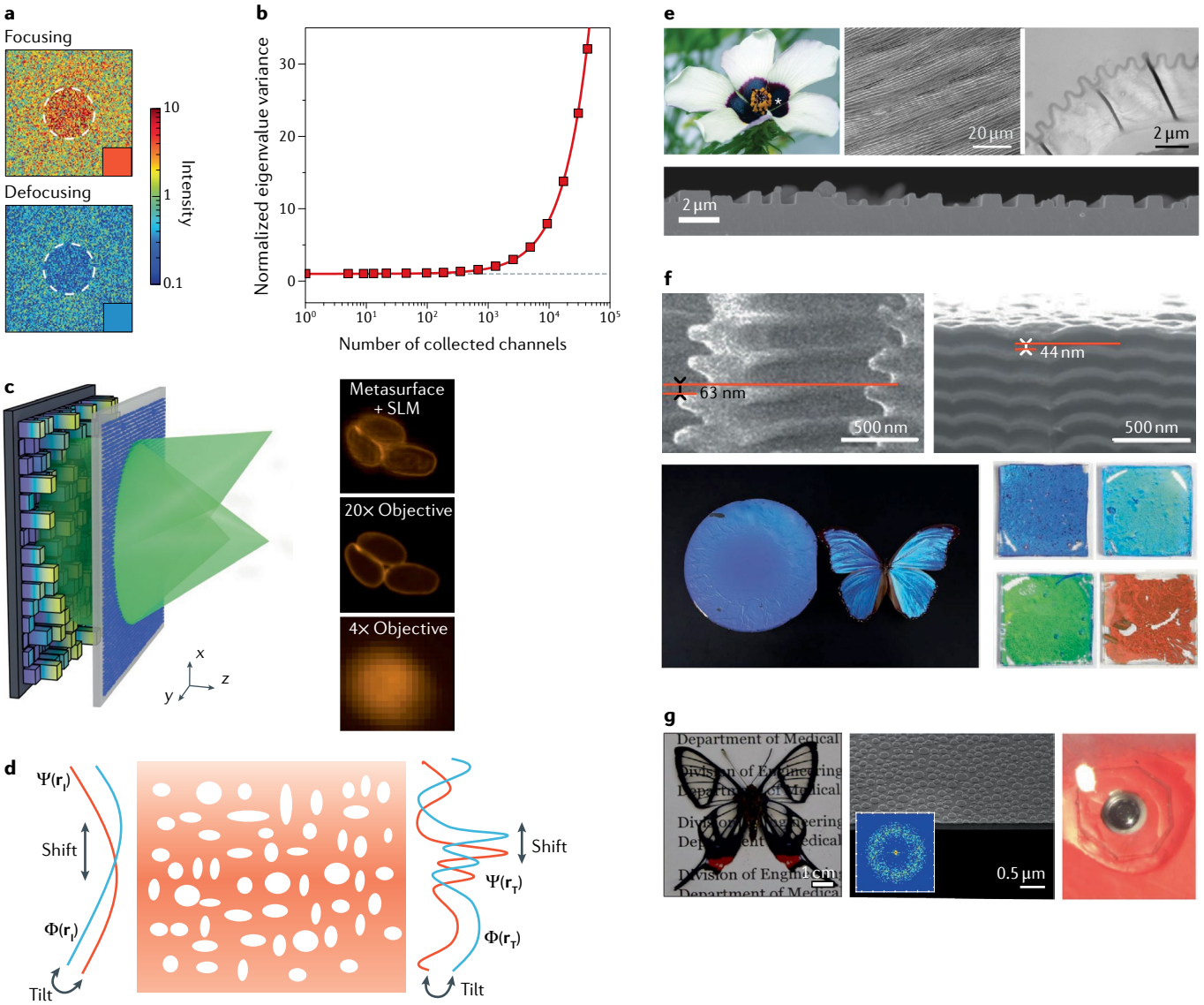

Fig. 7 | **Shaped wavefront and controlled directivity obtained with engineered disorder. a** | Maximal (top) and minimal (bottom) transmission into a target region containing 1,700 speckles, obtained by optimizing the light's wavefront[122]. The colour of the square on the corner of each image indicates the average intensity inside the target. **b** | The enhanced range of control obtained by controlling correlations[122]. For large targets (with a number of channels $M_2 \geq 10^3$), the range of control, as characterized by the variance of the eigenvalues of the transmission matrix, substantially increases. The illumination spot size is 6 µm. **c** | Broadband wavefront shaping assisted by disorder-engineered metasurfaces[127]. The insets show the application of this strategy to the high-resolution fluorescence imaging[127] of *Giardia lamblia* cysts, presenting a metasurface-assisted image (top), a ground-truth image with a 20× objective lens (middle) and an image with a 4× objective lens (bottom). **d** | Optical memory effect. The change of the input wavefront (from $\Psi(\mathbf{r}_I)$ to $\Phi(\mathbf{r}_I)$ at the position $\mathbf{r}_I$) leads to a correlated change in the output wavefront (from $\Psi(\mathbf{r}_T)$ to $\Phi(\mathbf{r}_T)$ at the position $\mathbf{r}_T$). This correlation can be calculated by using the original and changed transmission matrices[130]. **e** | The angiosperm *Hibiscus trionum*: the flower (left), a scanning electron microscopy (SEM) image (middle) and a transmission electron microscopy image (right). A flower-mimetic disordered grating with two height levels is shown in the lower part of the panel[132]. **f** | *Morpho didius* butterfly and its artificial realization: SEM images of a butterfly wing (left) and of a sample with engineered disorder mimicking it (right), and pictures of the resulting films encased in polydimethylsiloxane realizing different colours, depending on the vertical periodicities (bottom). The blue film is shown next to *M. didius* for comparison[133]. **g** | *Chorinea faunus* butterfly and its artificial realization: photo of a *C. faunus* butterfly under visible light (left); SEM image of the bio-inspired nanostructures (middle), with the inset showing the ring-shaped 2D Fourier power spectrum, which indicates a short-range order with a mean period of 445 ± 60 nm; and the application of the transparent film in an in vivo intraocular pressure sensor (right)[134]. SLM, spatial light modulator. Panels **a** and **b** are adapted from REF.[122], Springer Nature Limited. Panel **c** reprinted from REF.[127], Springer Nature Limited. Panel **e** reprinted from REF.[132], Springer Nature Limited. Panel **f** reprinted with permission from REF.[133], Wiley. Panel **g** reprinted from REF.[134], Springer Nature Limited.

monolayer of silica microspheres. The random distribution of the silica microspheres imposes a 3D random perturbation on the alternating layers while preserving the periodicity along the deposition axis (TABLE 1). These biomimetic structures exhibit superior colour quality compared with natural butterflies.

Recently, the wing of the *Chorinea faunus* butterfly was studied for the design of transparent disordered films[134] (FIG. 7g, left). In the butterfly, the transparent colour is due to nanostructures with short-range order, which provided the inspiration for a disordered film with low aspect ratio, isotropic scattering and enhanced omnidirectional transmission for the in vivo sensing of intraocular pressure (FIG. 7g, middle and right). Finally, the wing-scale structure of the butterfly *Pseudolycaena marsyas* was investigated[135] by quantifying its internal structural similarity to a random network, revealing that substantial amorphous gyroid microstructures play a critical role in determining the reflection spectrum. Apart from mimicking functionalities found in nature, an important focus of this type of research is understanding whether a certain biological structure produced by evolution is the optimized solution for a target functionality.

Disordered topological photonics

The use of topological concepts, which describe properties that are invariant under continuous deformations of a mathematical or physical object, has provided new design principles in condensed-matter physics, photonics, acoustics, microwaves and cold atoms. In photonics, the investigation and utilization of the topology of the dispersion bands has become a major research focus[10], with the aim of achieving topologically protected modes. Because the topology-dependent properties of these modes, such as the propagation direction, are protected against continuous deformations of the system, several exotic phenomena have been observed in photonic topological systems, including disorder-robust light propagation and photonic spin–orbit interactions.

Traditional research in disordered photonics has focused on classical optical quantities: frequencies, transport, wavefront and directivity of light. In line with the recent attention on topological quantities[10], disordered photonics have yielded new design methodologies that produce geometric or topological properties and spin or orbital angular momenta of light in the unexplored regime of broken translational order. In this section, we introduce recent reports on engineered disorder that interacts with the topological properties of light, including the effect of weak disorder on photonic topological insulators (TIs), the utilization of strong disorder for photonic topological Anderson insulators (TAIs) and spin–orbit interactions in disordered structures.

Weak disorder in photonic topological insulators. Photonic TIs enable backscattering-free light guiding by exploiting the topological nature of their eigenmodes. To generalize defect-immune light behaviours of TIs, detailed studies of the connection between disordered photonics and topological photonics are necessary, such as the manipulation of topological properties by engineering the strength and pattern of disorder[136,137]. However, the study of topology in disordered platforms has suffered from the lack of a proper topologically invariant quantity, because the widely used quantity, the Chern number, usually requires well-defined band structures with the closed Brillouin zone of periodic systems.

The effect of weak disorder, which preserves the bandgaps of TIs, has been investigated in photonic TIs. Disorder-induced topological transitions were studied in photonic metamaterials[136]. Although robust surface states with backscattering-free transport were observed for fluctuations of the optical potentials of up to 60%, a sudden topological transition accompanied by the emergence of localized hot spots was also revealed, which originates from Anderson localization (FIG. 8a). In this work, an empirical parameter measuring the confinement of surface states near the topological interface was used to identify the abrupt topological transition according to the increase of disorder strength. This empirical parameter was also used in recent work on topological states in amorphous photonic lattices[138], which demonstrated topological protection in photonic structures with short-range order. Assuming a very weak level of disorder, the concept of perturbative metamaterials[139] was suggested for the systematic design of TIs (FIG. 8b), resulting in the emergence of topological surface phonons.

In future work, it will be worth paying attention to the lifting of the restrictions on the Chern number afforded by its generalized definition first suggested by Kitaev[140]. This generalized quantity is constructed with the projection operator that describes the vibrations of the system, allowing for the real-space quantification of topological invariants. The proposed method has been applied to the realization of TIs in amorphous structures[141,142] and will accelerate the connection between disordered photonics and topological photonics.

Strong disorder for photonic topological Anderson insulators. The effect of strong disorder on TIs, almost closing the bandgaps, has drawn attention to the photonic realization[137,143] of TAIs[144]. Exposing the dramatic impact of topology on disordered photonics, the realization of a TAI implies the transition from an insulating state to a state with quantized conductance through the inclusion of sufficiently strong impurities in a 2D material. In contrast to an ordinary Anderson insulator that exhibits a monotonically suppressed conductance with increasing disorder, a TAI displays a disorder-induced emergence of the conductance[145]. The TAI conductance is also distinct from the protected conductance of a TI in the presence of disorder.

Effective lattices for the dynamical realization of TAIs were proposed[143] (FIG. 8c). First, the application of a time-varying gauge field to a honeycomb lattice leads to a bandgap with topologically protected edge states, forming TIs with time-reversal symmetry breaking. Then, with the subsequent breaking of inversion symmetry with detuned sublattices in the form of a staggered potential (red and green colouring in FIG. 8c), the band structure becomes topologically trivial. The introduction

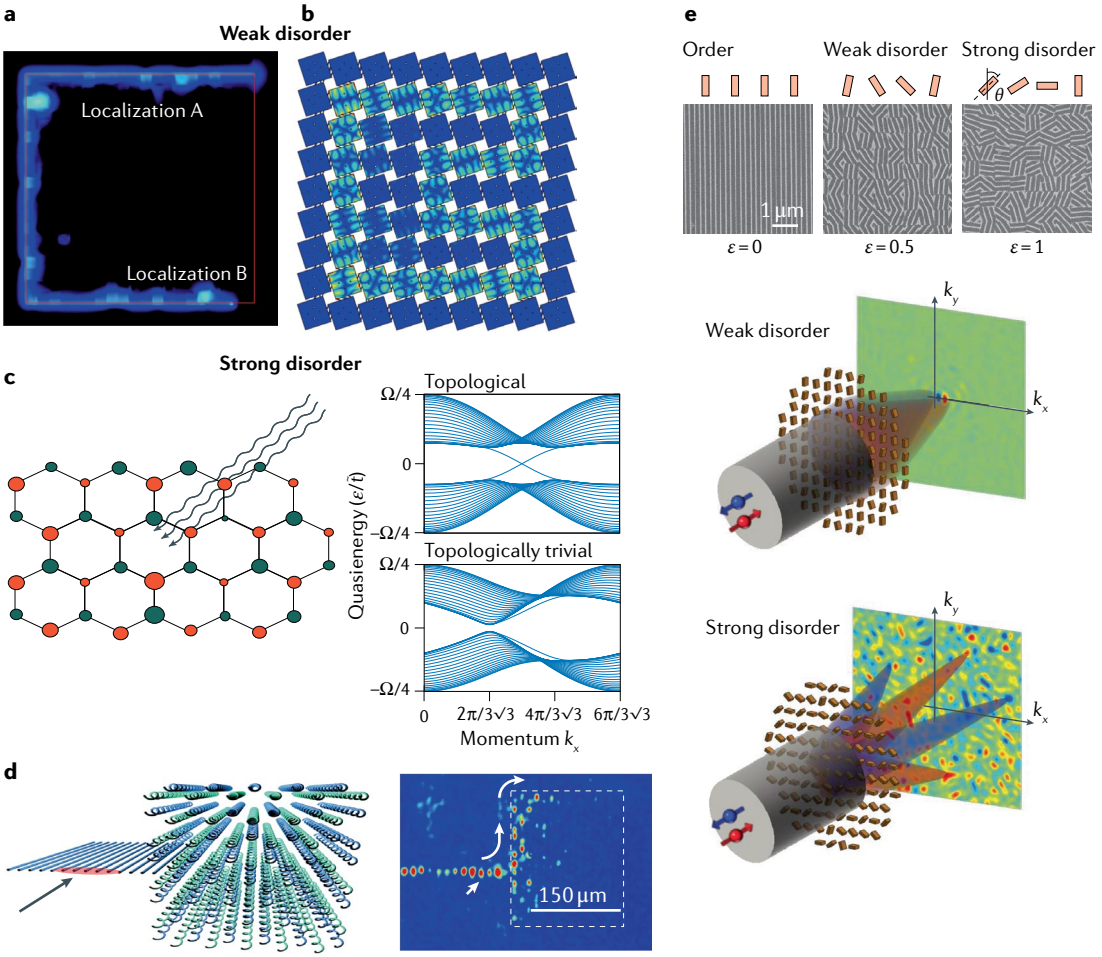

Fig. 8 | **Topological phenomena engineered by structural disorder. a**,**b** | Photonic topological insulator (TI) with weak disorder. **a** | Wave propagation inside a photonic TI with structural disorder, exhibiting topological state transitions[136]. **b** | TI designed using the mass-spring model[139]. For a metamaterial composed of weakly interacting unit cells, this model with the Schrieffer–Wolff transformation[160] allows the inverse design of metamaterial functionalities. **c**,**d** | Photonic topological Anderson insulator (TAI) with strong disorder. **c** | The dynamical realization of a TAI and its band diagrams[143]. The system is composed of a uniformly disordered graphene layer in the presence of a staggered mass potential and of circularly polarized light. Without the staggered potential and disorder, the circularly polarized light leads to the TI band structure. The introduction of the staggered mass potential (about 7% of the light frequency) into the TI phase results in a transition to the topologically trivial phase with inversion-symmetry breaking. Applying on-site disorder to this trivial state results in the TAI phase. **d** | A schematic of the experimental platform that realizes a TAI (left) and the measured TAI edge-state excitation (right)[137]. The 2D TAI system in panel **c** is reproduced with a 3D photonic structure by implementing the vector potential that originates from helical structures along the *z*-axis. The white dashed rectangle (right) indicates the photonic TAI, and the light arriving from outside is channelled in the edge state. **e** | Photonic spin–orbit interactions. Scanning electron microscopy images of silicon-based metasurface platforms with different strengths of disorder ε (top). The transition from weak to strong disorder[146] (middle and bottom, respectively) is accompanied by an abrupt change in photonic spin splitting. Panel **a** reprinted with permission from REF.[136], APS. Panel **b** reprinted from REF.[139], Springer Nature Limited. Panel **c** reprinted with permission from REF.[143], APS. Panel **d** adapted from REF.[137], Springer Nature Limited. Panel **e** reprinted with permission from REF.[146], AAAS.

of strong on-site disorder (different radii in FIG. 8c) then suppresses this inversion-symmetry breaking, recovering a topologically nontrivial phase and, thus, achieving gapless edge modes. A TAI was experimentally demonstrated in a static photonic platform using an array of helical coupled waveguides with on-site disorder[137] (FIG. 8d). The enhanced transport through edge modes and the short localization length of the bulk modes in photonic TAIs (TABLE 1) show how the interaction between disorder and topology provides new design freedom in the field of engineered disorder.

Spin–orbit interactions in disordered photonics. The impact of disorder on another topological phenomenon, spin–orbit interactions, was investigated in photonic metasurfaces[146]. The employed metasurface comprised subwavelength nanoantennas with random orientations θ ranging from $-\varepsilon\pi/2$ to $\varepsilon\pi/2$, where ε is the disorder strength (FIG. 8e). Because the orientation of each nanoantenna contributes to the geometric phase stemming from polarization change[147], the metasurface composes a subwavelength-scale, disordered-geometric-phase structure. By increasing the strength of disorder, a transition

from a photonic spin Hall effect of spin splitting within a diffraction-limited area to a random optical Rashba effect with numerous spin-split modes was observed in momentum space. This configuration results in spin-symmetry breakdown $I_{\sigma+}(\mathbf{k}) \neq I_{\sigma-}(\mathbf{k})$ (where $I_{\sigma\pm}(\mathbf{k})$ is the measured momentum-space intensity of each spin), which is in contrast with expectations based on the effective medium theory. Recently, an extension of these results was reported by inserting random local deformations in the metasurface structures[148]. With high defect concentrations, a random Rashba effect was reported. By contrast, low defect concentrations led to a photonic analogue of the topological Hall effect, originating from a pair of singularities in the pseudo-magnetic field.

Outlook

We have reviewed cornerstones in the field of engineered disorder, which have enabled the independent and traditionally contradictory control of multiple wave quantities. As evidenced by the recent results summarized in this Review, engineered disorder extends the 'dimensionality' of design freedom for controlling wave quantities through distinct paths of light–matter interactions. Traditional research in disordered photonics has focused on '1D' design freedom: the control of a single wave quantity, such as bandgaps, localization length or angular spectra. By contrast, a set of wave quantities and their interactions with disordered structures have transformed the problem into a multifaceted one. Although most recent results have focused on the 2D design space, as described in FIG. 2 and TABLE 1, higher-dimensional degrees of freedom from multiple interrelated wave quantities will give access to more intriguing optical phenomena through the precise engineering of each optical quantity and their mixing.

On the theoretical side, interdisciplinary concepts inspired by related fields, such as hyperuniformity[60], chaos theory[53] and the de Broglie–Bohm theory[108], have provided a new perspective on the deterministic engineering of optical disorder. The regime of 'uniformity' is statistically generalized with the concept of hyperuniformity, grouping crystals, quasicrystals, aperiodic sequences and correlated disorder under a single umbrella. Chaotic channels enable a substantial increase in the optical path lengths in a given space, allowing for integrated photonic devices in disordered platforms. Bohmian formulations tackle the individual handling of wave phase and amplitude in complex optical potentials, connecting disordered photonics and non-Hermitian photonics. In addition, the concepts of synthetic dimensions[149] and time crystals[150] in ordered systems will provide vast and new regimes to explore in disordered photonics.

Recently developed fabrication and optimization techniques have enabled the realization of target disordered patterns. Extreme nanofabrication technologies[151] allow the precise and large-scale generation of engineered disordered patterns with top-down[5,64] or bottom-up[65,66] processes, such as the construction of hyperuniform structures using photolithography and 3D printing[52]. Self-assembly techniques also enable the precise control of short-range order in disordered structures, and have been applied to obtain enhanced Purcell factors in spontaneous emission[152] and tunable random lasing[153]. Machine-learning techniques[154–156], enabling the systematic modelling of the relationship between various wave quantities and their mixing in Maxwell's equations, are promising choices for the efficient numerical modelling of disordered light–matter interactions, as was shown in solid-state physics[156,157]. Conversely, because neural networks are correlated disordered systems with nonlinear activations, we can envisage the construction of complex optical networks composed of delicately engineered disordered structures with optical nonlinearity to improve the current light-based machine-learning process[158]. The exploration of the potential of disordered photonics has just begun and promises a variety of breakthroughs in both science and engineering.

Published online 9 December 2020

1. Hughes, S., Ramunno, L., Young, J. F. & Sipe, J. E. Extrinsic optical scattering loss in photonic crystal waveguides: role of fabrication disorder and photon group velocity. *Phys. Rev. Lett.* **94**, 033903 (2005).
2. Barabási, A.-L. *Network Science* (Cambridge Univ. Press, 2016).
3. Barabási, A.-L. & Albert, R. Emergence of scaling in random networks. *Science* **286**, 509–512 (1999).
4. Torquato, S. & Stillinger, F. H. Local density fluctuations, hyperuniformity, and order metrics. *Phys. Rev. E* **68**, 041113 (2003).
This work first introduced the concept of hyperuniformity, that is, the suppression of long-range fluctuations.
5. Man, W. et al. Isotropic band gaps and freeform waveguides observed in hyperuniform disordered photonic solids. *Proc. Natl Acad. Sci. USA* **110**, 15886–15891 (2013).
This paper experimentally measured the isotropic, complete bandgap in hyperuniform structures.
6. Goodrich, C. P., Liu, A. J. & Nagel, S. R. Solids between the mechanical extremes of order and disorder. *Nat. Phys.* **10**, 578–581 (2014).
7. Rayleigh, L. XVII. On the maintenance of vibrations by forces of double frequency, and on the propagation of waves through a medium endowed with a periodic structure. *Philos. Mag.* **24**, 145–159 (1887).
8. Joannopoulos, J. D., Johnson, S. G., Winn, J. N. & Meade, R. D. *Photonic Crystals: Molding the Flow of Light* (Princeton Univ. Press, 2011).
9. Vardeny, Z. V., Nahata, A. & Agrawal, A. Optics of photonic quasicrystals. *Nat. Photonics* **7**, 177–187 (2013).
10. Lu, L., Joannopoulos, J. D. & Soljačić, M. Topological photonics. *Nat. Photonics* **8**, 821–829 (2014).
11. Freedman, B. et al. Wave and defect dynamics in nonlinear photonic quasicrystals. *Nature* **440**, 1166–1169 (2006).
12. Lahini, Y. et al. Observation of a localization transition in quasiperiodic photonic lattices. *Phys. Rev. Lett.* **103**, 013901 (2009).
13. Wang, P. et al. Localization and delocalization of light in photonic moiré lattices. *Nature* **577**, 42–46 (2020).
14. Anderson, P. W. Absence of diffusion in certain random lattices. *Phys. Rev.* **109**, 1492 (1958).
15. John, S. Electromagnetic absorption in a disordered medium near a photon mobility edge. *Phys. Rev. Lett.* **53**, 2169 (1984).
16. Van Albada, M. P. & Lagendijk, A. Observation of weak localization of light in a random medium. *Phys. Rev. Lett.* **55**, 2692 (1985).
17. Anderson, P. W. The question of classical localization A theory of white paint? *Philos. Mag. B* **52**, 505–509 (1985).
18. John, S. Strong localization of photons in certain disordered dielectric superlattices. *Phys. Rev. Lett.* **58**, 2486 (1987).
19. Pursiainen, O. L. et al. Nanoparticle-tuned structural color from polymer opals. *Opt. Express* **15**, 9553–9561 (2007).
20. Saranathan, V. et al. Structure and optical function of amorphous photonic nanostructures from avian feather barbs: a comparative small angle X-ray scattering (SAXS) analysis of 230 bird species. *J. R. Soc. Interface* **9**, 2563–2580 (2012).
21. Vukusic, P. & Sambles, J. R. Photonic structures in biology. *Nature* **424**, 852–855 (2003).
22. Li, Z.-Y. & Zhang, Z.-Q. Fragility of photonic band gaps in inverse-opal photonic crystals. *Phys. Rev. B* **62**, 1516 (2000).
23. Sebbah, P. *Waves and Imaging Through Complex Media* (Springer, 2012).
24. Pratesi, F., Burresi, M., Riboli, F., Vynck, K. & Wiersma, D. S. Disordered photonic structures for light harvesting in solar cells. *Opt. Express* **21**, A460–A468 (2013).
25. Liu, J. et al. Random nanolasing in the Anderson localized regime. *Nat. Nanotechnol.* **9**, 285–289 (2014).
26. Wiersma, D. S. Disordered photonics. *Nat. Photonics* **7**, 188–196 (2013).
27. Rintoul, M. & Torquato, S. Metastability and crystallization in hard-sphere systems. *Phys. Rev. Lett.* **77**, 4198 (1996).
28. Torquato, S., Truskett, T. M. & Debenedetti, P. G. Is random close packing of spheres well defined? *Phys. Rev. Lett.* **84**, 2064 (2000).
29. Torquato, S. Perspective: basic understanding of condensed phases of matter via packing models. *J. Chem. Phys.* **149**, 020901 (2018).

30. Errington, J. R., Debenedetti, P. G. & Torquato, S. Quantification of order in the Lennard-Jones system. *J. Chem. Phys.* **118**, 2256–2263 (2003).
31. Zhang, G., Stillinger, F. & Torquato, S. The perfect glass paradigm: disordered hyperuniform glasses down to absolute zero. *Sci. Rep.* **6**, 36963 (2016).
32. Errington, J. R. & Debenedetti, P. G. Relationship between structural order and the anomalies of liquid water. *Nature* **409**, 318–321 (2001).
33. DiStasio, R. A. Jr, Zhang, G., Stillinger, F. H. & Torquato, S. Rational design of stealthy hyperuniform two-phase media with tunable order. *Phys. Rev. E* **97**, 023311 (2018).
34. Jiao, Y. et al. Avian photoreceptor patterns represent a disordered hyperuniform solution to a multiscale packing problem. *Phys. Rev. E* **89**, 022721 (2014).
35. Chen, D. & Torquato, S. Designing disordered hyperuniform two-phase materials with novel physical properties. *Acta Mater.* **142**, 152–161 (2018).
36. Shechtman, D., Blech, I., Gratias, D. & Cahn, J. W. Metallic phase with long-range orientational order and no translational symmetry. *Phys. Rev. Lett.* **53**, 1951 (1984).
37. Levine, D. & Steinhardt, P. J. Quasicrystals: a new class of ordered structures. *Phys. Rev. Lett.* **53**, 2477 (1984).
38. Kansal, A. R., Truskett, T. M. & Torquato, S. Nonequilibrium hard-disk packings with controlled orientational order. *J. Chem. Phys.* **113**, 4844–4851 (2000).
39. Steinhardt, P. J., Nelson, D. R. & Ronchetti, M. Bond-orientational order in liquids and glasses. *Phys. Rev. B* **28**, 784 (1983).
40. Torquato, S., Zhang, G. & Stillinger, F. Ensemble theory for stealthy hyperuniform disordered ground states. *Phys. Rev. X* **5**, 021020 (2015).
41. Zachary, C. E. & Torquato, S. Hyperuniformity in point patterns and two-phase random heterogeneous media. *J. Stat. Mech. Theory Exp.* **2009**, P12015 (2009).
42. Yu, S., Piao, X., Hong, J. & Park, N. Bloch-like waves in random-walk potentials based on supersymmetry. *Nat. Commun.* **6**, 8269 (2015).
43. Torquato, S. *Random Heterogeneous Materials: Microstructure and Macroscopic Properties* (Springer, 2002).
44. Torquato, S., Zhang, G. & De Courcy-Ireland, M. Hidden multiscale order in the primes. *J. Phys. A* **52**, 135002 (2019).
45. Klatt, M. A., Kim, J. & Torquato, S. Cloaking the underlying long-range order of randomly perturbed lattices. *Phys. Rev. E* **101**, 032118 (2020).
46. Jiang, X. et al. Chaos-assisted broadband momentum transformation in optical microresonators. *Science* **358**, 344–347 (2017).
This paper presented a strategy to overcome the traditional bandwidth limitation in evanescent coupling methods by exploiting dynamical tunnelling.
47. Florescu, M., Torquato, S. & Steinhardt, P. J. Designer disordered materials with large, complete photonic band gaps. *Proc. Natl Acad. Sci. USA* **106**, 20658–20663 (2009).
48. Hsu, C. W., Goetschy, A., Bromberg, Y., Stone, A. D. & Cao, H. Broadband coherent enhancement of transmission and absorption in disordered media. *Phys. Rev. Lett.* **115**, 223901 (2015).
49. Bigourdan, F., Pierrat, R. & Carminati, R. Enhanced absorption of waves in stealth hyperuniform disordered media. *Opt. Express* **27**, 8666–8682 (2019).
50. Batten, R. D., Stillinger, F. H. & Torquato, S. Classical disordered ground states: super-ideal gases and stealth and equi-luminous materials. *J. Appl. Phys.* **104**, 033504 (2008).
51. Klatt, M. A. et al. Universal hidden order in amorphous cellular geometries. *Nat. Commun.* **10**, 811 (2019).
52. Kim, J. & Torquato, S. C. New tessellation-based procedure to design perfectly hyperuniform disordered dispersions for materials discovery. *Acta Mater.* **168**, 143–151 (2019).
53. Cao, H. & Wiersig, J. Dielectric microcavities: model systems for wave chaos and non-Hermitian physics. *Rev. Mod. Phys.* **87**, 61 (2015).
54. Kellert, S. H. *In the Wake of Chaos: Unpredictable Order in Dynamical Systems* (Univ. Chicago Press, 1993).
55. Bäcker, A. et al. Dynamical tunneling in mushroom billiards. *Phys. Rev. Lett.* **100**, 174103 (2008).
56. Bittner, S. et al. Suppressing spatiotemporal lasing instabilities with wave-chaotic microcavities. *Science* **361**, 1225–1231 (2018).
57. Yi, C.-H., Kullig, J. & Wiersig, J. Pair of exceptional points in a microdisk cavity under an extremely weak deformation. *Phys. Rev. Lett.* **120**, 093902 (2018).
This paper showed that even a very weak deformation in a microdisk can lead to the emergence of exceptional points.
58. Miri, M.-A. & Alù, A. Exceptional points in optics and photonics. *Science* **363**, eaar7709 (2019).
59. Kim, Y. et al. Designing whispering gallery modes via transformation optics. *Nat. Photonics* **10**, 647–652 (2016).
60. Torquato, S. Hyperuniform states of matter. *Phys. Rep.* **745**, 1–95 (2018).
61. Uche, O. U., Stillinger, F. H. & Torquato, S. Constraints on collective density variables: two dimensions. *Phys. Rev. E* **70**, 046122 (2004).
62. Leseur, O., Pierrat, R. & Carminati, R. High-density hyperuniform materials can be transparent. *Optica* **3**, 763–767 (2016).
63. Froufe-Pérez, L. S. et al. Role of short-range order and hyperuniformity in the formation of band gaps in disordered photonic materials. *Phys. Rev. Lett.* **117**, 053902 (2016).
64. Muller, N., Haberko, J., Marichy, C. & Scheffold, F. Photonic hyperuniform networks obtained by silicon double inversion of polymer templates. *Optica* **4**, 361–366 (2017).
65. Ma, T. et al. 3D printed hollow-core terahertz optical waveguides with hyperuniform disordered dielectric reflectors. *Adv. Opt. Mater.* **4**, 2085–2094 (2016).
66. Piechulla, P. M. et al. Fabrication of nearly-hyperuniform substrates by tailored disorder for photonic applications. *Adv. Opt. Mater.* **6**, 1701272 (2018).
67. Kac, M. Can one hear the shape of a drum? *Am. Math. Monthly* **73**, 1–23 (1966).
68. Gordon, C., Webb, D. L. & Wolpert, S. One cannot hear the shape of a drum. *Bull. Am. Math. Soc.* **27**, 134–138 (1992).
69. Miri, M.-A., Heinrich, M., El-Ganainy, R. & Christodoulides, D. N. Supersymmetric optical structures. *Phys. Rev. Lett.* **110**, 233902 (2013).
70. Heinrich, M. et al. Supersymmetric mode converters. *Nat. Commun.* **5**, 3698 (2014).
71. Hokmabadi, M. P., Nye, N. S., El-Ganainy, R., Christodoulides, D. N. & Khajavikhan, M. Supersymmetric laser arrays. *Science* **363**, 623–626 (2019).
72. Longhi, S. Bloch oscillations in tight-binding lattices with defects. *Phys. Rev. B* **81**, 195118 (2010).
73. Teimourpour, M., Christodoulides, D. N. & El-Ganainy, R. Optical revivals in nonuniform supersymmetric photonic arrays. *Opt. Lett.* **41**, 372–375 (2016).
74. Miri, M.-A., Heinrich, M. & Christodoulides, D. N. Supersymmetry-generated complex optical potentials with real spectra. *Phys. Rev. A* **87**, 043819 (2013).
75. Miri, M.-A., Heinrich, M. & Christodoulides, D. N. SUSY-inspired one-dimensional transformation optics. *Optica* **1**, 89–95 (2014).
76. Zhong, Q., Nelson, S., Khajavikhan, M., Christodoulides, D. & El-Ganainy, R. Bosonic discrete supersymmetry for quasi-two-dimensional optical arrays. *Photonics Res.* **7**, 1240–1243 (2019).
77. Yu, S., Piao, X., Hong, J. & Park, N. Interdimensional optical isospectrality inspired by graph networks. *Optica* **3**, 836–839 (2016).
78. Teimourpour, M. H., Ge, L., Christodoulides, D. N. & El-Ganainy, R. Non-Hermitian engineering of single mode two dimensional laser arrays. *Sci. Rep.* **6**, 33253 (2016).
79. Maczewsky, L. J. et al. Synthesizing multi-dimensional excitation dynamics and localization transition in one-dimensional lattices. *Nat. Photonics* **14**, 76–81 (2020).
80. Abrahams, E., Anderson, P., Licciardello, D. & Ramakrishnan, T. Scaling theory of localization: absence of quantum diffusion in two dimensions. *Phys. Rev. Lett.* **42**, 673 (1979).
81. Sheng, P. *Introduction to Wave Scattering, Localization and Mesoscopic Phenomena* (Springer, 2006).
82. Segev, M., Silberberg, Y. & Christodoulides, D. N. Anderson localization of light. *Nat. Photonics* **7**, 197–204 (2013).
83. De Raedt, H., Lagendijk, A. & de Vries, P. Transverse localization of light. *Phys. Rev. Lett.* **62**, 47 (1989).
This paper first predicted the transverse localization of light.
84. Chabanov, A., Stoytchev, M. & Genack, A. Statistical signatures of photon localization. *Nature* **404**, 850–853 (2000).
This paper reported the landmark observation of microwave localization in a quasi-1D geometry.
85. Lahini, Y. et al. Anderson localization and nonlinearity in one-dimensional disordered photonic lattices. *Phys. Rev. Lett.* **100**, 013906 (2008).
86. Szameit, A. et al. Wave localization at the boundary of disordered photonic lattices. *Opt. Lett.* **35**, 1172–1174 (2010).
87. Pertsch, T. et al. Nonlinearity and disorder in fiber arrays. *Phys. Rev. Lett.* **93**, 053901 (2004).
88. Schwartz, T., Bartal, G., Fishman, S. & Segev, M. Transport and Anderson localization in disordered two-dimensional photonic lattices. *Nature* **446**, 52–55 (2007).
89. Skipetrov, S. & Page, J. H. Red light for Anderson localization. *New J. Phys.* **18**, 021001 (2016).
90. Choi, S. H. et al. Anderson light localization in biological nanostructures of native silk. *Nat. Commun.* **9**, 452 (2018).
91. Leonetti, M., Karbasi, S., Mafi, A. & Conti, C. Light focusing in the Anderson regime. *Nat. Commun.* **5**, 4534 (2014).
92. Ruocco, G., Abaie, B., Schirmacher, W., Mafi, A. & Leonetti, M. Disorder-induced single-mode transmission. *Nat. Commun.* **8**, 14571 (2017).
93. Gaio, M. et al. A nanophotonic laser on a graph. *Nat. Commun.* **10**, 226 (2019).
94. Niklasson, G. A., Granqvist, C. & Hunderi, O. Effective medium models for the optical properties of inhomogeneous materials. *Appl. Opt.* **20**, 26–30 (1981).
95. Sheinfux, H. H., Kaminer, I., Plotnik, Y., Bartal, G. & Segev, M. Subwavelength multilayer dielectrics: ultrasensitive transmission and breakdown of effective-medium theory. *Phys. Rev. Lett.* **113**, 243901 (2014).
96. Sheinfux, H. H., Kaminer, I., Genack, A. Z. & Segev, M. Interplay between evanescence and disorder in deep subwavelength photonic structures. *Nat. Commun.* **7**, 12927 (2016).
This study theoretically demonstrated the emergence of measurable transverse Anderson localization in deep-subwavelength optical structures.
97. Sheinfux, H. H. et al. Observation of Anderson localization in disordered nanophotonic structures. *Science* **356**, 953–956 (2017).
98. Zhang, Z.-Q. & Sheng, P. Superdiffusive transport and metal-insulator transition in two dimensions. *Phys. Rev. Lett.* **67**, 2541 (1991).
99. Xue, W., Sheng, P., Chu, Q.-J. & Zhang, Z.-Q. Localization transition in media with anisotropic diagonal disorder. *Phys. Rev. Lett.* **63**, 2837 (1989).
100. Feng, L., El-Ganainy, R. & Ge, L. Non-Hermitian photonics based on parity–time symmetry. *Nat. Photonics* **11**, 752–762 (2017).
101. Barthelemy, P., Bertolotti, J. & Wiersma, D. S. A Lévy flight for light. *Nature* **453**, 495–498 (2008).
This paper first demonstrated the engineering of optical materials to achieve light waves that realize a Lévy flight.
102. Bertolotti, J. et al. Engineering disorder in superdiffusive Levy glasses. *Adv. Funct. Mater.* **20**, 965–968 (2010).
103. Burresi, M. et al. Weak localization of light in superdiffusive random systems. *Phys. Rev. Lett.* **108**, 110604 (2012).
104. Conley, G. M., Burresi, M., Pratesi, F., Vynck, K. & Wiersma, D. S. Light transport and localization in two-dimensional correlated disorder. *Phys. Rev. Lett.* **112**, 143901 (2014).
105. Makris, K. G., Musslimani, Z. H., Christodoulides, D. N. & Rotter, S. Constant-intensity waves and their modulation instability in non-Hermitian potentials. *Nat. Commun.* **6**, 7257 (2015).
106. Yu, S., Piao, X., Hong, J. & Park, N. Metadisorder for designer light in random systems. *Sci. Adv.* **2**, e1501851 (2016).
107. Makris, K. G., Brandstötter, A., Ambichl, P., Musslimani, Z. H. & Rotter, S. Wave propagation through disordered media without backscattering and intensity variations. *Light Sci. Appl.* **6**, e17035 (2017).
108. Yu, S., Piao, X. & Park, N. Bohmian photonics for independent control of the phase and amplitude of waves. *Phys. Rev. Lett.* **120**, 193902 (2018).
109. Brandstötter, A., Makris, K. G. & Rotter, S. Scattering-free pulse propagation through invisible non-Hermitian media. *Phys. Rev. B* **99**, 115402 (2019).
110. Hatano, N. & Nelson, D. R. Localization transitions in non-Hermitian quantum mechanics. *Phys. Rev. Lett.* **77**, 570 (1996).
111. Kildishev, A. V., Boltasseva, A. & Shalaev, V. M. Planar photonics with metasurfaces. *Science* **339**, 1232009 (2013).

112. Mosk, A. P., Lagendijk, A., Lerosey, G. & Fink, M. Controlling waves in space and time for imaging and focusing in complex media. *Nat. Photonics* **6**, 283–292 (2012).
113. Vellekoop, I. M. & Mosk, A. Focusing coherent light through opaque strongly scattering media. *Opt. Lett.* **32**, 2309–2311 (2007).
This paper first suggested the use of wavefront shaping for designed focusing through disordered media.
114. Popoff, S. et al. Measuring the transmission matrix in optics: an approach to the study and control of light propagation in disordered media. *Phys. Rev. Lett.* **104**, 100601 (2010).
This paper first realized wavefront shaping through the experimental measurement of the transmission matrix.
115. Huang, Y.-F., Jen, Y.-J., Chen, L.-C., Chen, K.-H. & Chattopadhyay, S. Design for approaching cicada-wing reflectance in low-and high-index biomimetic nanostructures. *ACS Nano* **9**, 301–311 (2015).
116. McCoy, D. E., Feo, T., Harvey, T. A. & Prum, R. O. Structural absorption by barbule microstructures of super black bird of paradise feathers. *Nat. Commun.* **9**, 1 (2018).
117. Freund, I. Looking through walls and around corners. *Phys. A Stat. Mech. Appl.* **168**, 49–65 (1990).
118. Vellekoop, I. M., Lagendijk, A. & Mosk, A. Exploiting disorder for perfect focusing. *Nat. Photonics* **4**, 320–322 (2010).
This cornerstone paper demonstrated the increase of the numerical aperture in disordered materials.
119. Horstmeyer, R., Ruan, H. & Yang, C. Guidestar-assisted wavefront-shaping methods for focusing light into biological tissue. *Nat. Photonics* **9**, 563–571 (2015).
120. Rotter, S. & Gigan, S. Light fields in complex media: mesoscopic scattering meets wave control. *Rev. Mod. Phys.* **89**, 015005 (2017).
This review provides a solid theoretical background on wavefront shaping.
121. Lee, P. A. & Stone, A. D. Universal conductance fluctuations in metals. *Phys. Rev. Lett.* **55**, 1622 (1985).
122. Hsu, C. W., Liew, S. F., Goetschy, A., Cao, H. & Stone, A. D. Correlation-enhanced control of wave focusing in disordered media. *Nat. Phys.* **13**, 497–502 (2017).
123. Derode, A., Roux, P. & Fink, M. Robust acoustic time reversal with high-order multiple scattering. *Phys. Rev. Lett.* **75**, 4206 (1995).
124. Lerosey, G., De Rosny, J., Tourin, A. & Fink, M. Focusing beyond the diffraction limit with far-field time reversal. *Science* **315**, 1120–1122 (2007).
125. Choi, Y. et al. Overcoming the diffraction limit using multiple light scattering in a highly disordered medium. *Phys. Rev. Lett.* **107**, 023902 (2011).
126. Van Putten, E. et al. Scattering lens resolves sub-100 nm structures with visible light. *Phys. Rev. Lett.* **106**, 193905 (2011).
127. Jang, M. et al. Wavefront shaping with disorder-engineered metasurfaces. *Nat. Photonics* **12**, 84–90 (2018).
128. Feng, S., Kane, C., Lee, P. A. & Stone, A. D. Correlations and fluctuations of coherent wave transmission through disordered media. *Phys. Rev. Lett.* **61**, 834 (1988).
129. Judkewitz, B., Horstmeyer, R., Vellekoop, I. M., Papadopoulos, I. N. & Yang, C. Translation correlations in anisotropically scattering media. *Nat. Phys.* **11**, 684–689 (2015).
130. Osnabrugge, G., Horstmeyer, R., Papadopoulos, I. N., Judkewitz, B. & Vellekoop, I. M. Generalized optical memory effect. *Optica* **4**, 886–892 (2017).
This paper provided an analytical framework for generalized optical memory effects, including 'tilt' and 'shift' functions and their interactions.
131. Wilts, B. D. et al. Evolutionary-optimized photonic network structure in white beetle wing scales. *Adv. Mater.* **30**, 1702057 (2018).
132. Moyroud, E. et al. Disorder in convergent floral nanostructures enhances signalling to bees. *Nature* **550**, 469–474 (2017).
This paper demonstrated the critical role of disordered photonic structures in biology.
133. Chung, K. et al. Flexible, angle-independent, structural color reflectors inspired by Morpho butterfly wings. *Adv. Mater.* **24**, 2375–2379 (2012).
134. Narasimhan, V. et al. Multifunctional biophotonic nanostructures inspired by the longtail glasswing butterfly for medical devices. *Nat. Nanotechnol.* **13**, 512–519 (2018).
135. Sellers, S. R., Man, W., Sahba, S. & Florescu, M. Local self-uniformity in photonic networks. *Nat. Commun.* **8**, 14439 (2017).
136. Liu, C., Gao, W., Yang, B. & Zhang, S. Disorder-induced topological state transition in photonic metamaterials. *Phys. Rev. Lett.* **119**, 183901 (2017).
This work reported disorder-induced topological transitions in photonic metamaterials using an empirical parameter.
137. Stützer, S. et al. Photonic topological Anderson insulators. *Nature* **560**, 461–465 (2018).
138. Yang, B. et al. Topological states in amorphous magnetic photonic lattices. *Phys. Rev. B* **99**, 045307 (2019).
139. Matlack, K. H., Serra-Garcia, M., Palermo, A., Huber, S. D. & Daraio, C. Designing perturbative metamaterials from discrete models. *Nat. Mater.* **17**, 323–328 (2018).
140. Kitaev, A. Anyons in an exactly solved model and beyond. *Ann. Phys.* **321**, 2–111 (2006).
141. Agarwala, A. & Shenoy, V. B. Topological insulators in amorphous systems. *Phys. Rev. Lett.* **118**, 236402 (2017).
142. Mitchell, N. P., Nash, L. M., Hexner, D., Turner, A. M. & Irvine, W. T. Amorphous topological insulators constructed from random point sets. *Nat. Phys.* **14**, 380–385 (2018).
143. Titum, P., Lindner, N. H., Rechtsman, M. C. & Refael, G. Disorder-induced Floquet topological insulators. *Phys. Rev. Lett.* **114**, 056801 (2015).
144. Li, J., Chu, R.-L., Jain, J. & Shen, S.-Q. Topological Anderson insulator. *Phys. Rev. Lett.* **102**, 136806 (2009).
145. Groth, C., Wimmer, M., Akhmerov, A., Tworzydło, J. & Beenakker, C. Theory of the topological Anderson insulator. *Phys. Rev. Lett.* **103**, 196805 (2009).
146. Maguid, E. et al. Disorder-induced optical transition from spin Hall to random Rashba effect. *Science* **358**, 1411–1415 (2017).
This work reported spin-optical transport phenomena arising from a disordered geometric phase in subwavelength optical structures.
147. Mueller, J. B., Rubin, N. A., Devlin, R. C., Groever, B. & Capasso, F. Metasurface polarization optics: independent phase control of arbitrary orthogonal states of polarization. *Phys. Rev. Lett.* **118**, 113901 (2017).
148. Wang, B. et al. Photonic topological spin Hall effect mediated by vortex pairs. *Phys. Rev. Lett.* **123**, 266101 (2019).
149. Lustig, E. et al. Photonic topological insulator in synthetic dimensions. *Nature* **567**, 356–360 (2019).
150. Zhang, J. et al. Observation of a discrete time crystal. *Nature* **543**, 217–220 (2017).
151. Shirazi, S. F. S. et al. A review on powder-based additive manufacturing for tissue engineering: selective laser sintering and inkjet 3D printing. *Sci. Technol. Adv. Mater.* **16**, 033502 (2015).
152. Sapienza, R. et al. Long-tail statistics of the purcell factor in disordered media driven by near-field interactions. *Phys. Rev. Lett.* **106**, 163902 (2011).
153. García, P. D., Sapienza, R. & López, C. Photonic glasses: a step beyond white paint. *Adv. Mater.* **22**, 12–19 (2010).
154. Liu, D., Tan, Y., Khoram, E. & Yu, Z. Training deep neural networks for the inverse design of nanophotonic structures. *ACS Photonics* **5**, 1365–1369 (2018).
155. Ma, W., Cheng, F. & Liu, Y. Deep-learning-enabled on-demand design of chiral metamaterials. *ACS Nano* **12**, 6326–6334 (2018).
156. Yu, S., Piao, X. & Park, N. Machine learning identifies scale-free properties in disordered materials. *Nat. Commun.* **11**, 4842 (2020).
157. Cubuk, E. D. et al. Identifying structural flow defects in disordered solids using machine-learning methods. *Phys. Rev. Lett.* **114**, 108001 (2015).
158. Shen, Y. et al. Deep learning with coherent nanophotonic circuits. *Nat. Photonics* **11**, 441–446 (2017).
159. Levi, L., Krivolapov, Y., Fishman, S. & Segev, M. Hyper-transport of light and stochastic acceleration by evolving disorder. *Nat. Phys.* **8**, 912–917 (2012).
160. Bravyi, S., DiVincenzo, D. P. & Loss, D. Schrieffer–Wolff transformation for quantum many-body systems. *Ann. Phys.* **326**, 2793–2826 (2011).

Acknowledgements
The authors thank M. Klatt, J. Kim, T. Middlemas and C. Maher for their helpful suggestions on the manuscript. S. Yu and N. Park acknowledge financial support from the National Research Foundation of Korea (NRF) through the Global Frontier Program (2014M3A6B3063708). S. Yu was also supported by the Basic Science Research Program (2016R1A6A3A04009723). C.-W.Q. acknowledges financial support from the National Research Foundation, Prime Minister's Office, Singapore under its Competitive Research Program (CRP award NRF-CRP15-2015-03). S. Torquato was supported by the Princeton University Innovation Fund for New Ideas in the Natural Sciences.

Author contributions
All authors contributed to the final manuscript.

Competing interests
The authors have no conflicts of interest to declare.

Publisher's note
Springer Nature remains neutral with regard to jurisdictional claims in published maps and institutional affiliations.